RNA-triggered fluorescence controlled by RNA switches for real-time RNA expression tracking in living plants

Jiuyuan Bai[1,2]†, Yazhou Chen[3,4]†, Jiayu Zhang[1], Jiang Li[5], Hongpei Ren[1], Shan Pan[1], Yiran Tao[1], Miaomiao Lei[1], Mengyue Dong[1], Sha Liu[1], Jia Yi[1], Fang Chen[1], Chunhai Fan[6]*, Yun Zhao[1]*

Affiliations:

[1]Key Laboratory of Bio-Resource and Eco-Environment of Ministry of Education, College of Life Sciences, Sichuan University, Chengdu 610065, China.

[2]Microbiology and Metabolic Engineering Key Laboratory of Sichuan Province, College of Life Sciences, Sichuan University, Chengdu 610065, China.

[3]Hubei Hongshan Laboratory, Wuhan, 430070, China;

[4]Hubei Insect Resources Utilization and Sustainable Pest Management Key Laboratory, College of Plant Science and Technology, Huazhong Agricultural University, Wuhan, 430070, China;

[5]Institute of Materiobiology, College of Sciences, Shanghai University, Shanghai 200444, China.

[6]Institute of Translational Medicine, Shanghai Jiao Tong University, Shanghai 200240, China.

†J.B. and Y.C. contributed equally to this work.

*Corresponding author. Email: fanchunhai@sjtu.edu.cn; zhaoyun@scu.edu.cn

Abstract

Tracking RNA expression dynamics in living plants is critical for understanding gene regulation, yet real-time visualization remains a significant challenge. We have addressed this issue by *de novo* engineering an RNA-triggered fluorescence (RTF) reporter system precisely controlled by programmable RNA switches and achieved dynamic imaging of RNA expression at the cellular level and the whole-plant scale. The RNA switch-RTF system enabled the dynamic real-time tracking of developmentally regulated, tissue-specific, circadian, and stress-responsive mRNAs, as well as the movement of a mobile mRNA and an aphid-secreted cross-kingdom long non-coding RNA. By providing a powerful platform for real-time RNA imaging *in vivo*, our approach opens new avenues for studying gene regulation, signaling, and mobility in plants, with potential applications in synthetic biology and crop improvement.

Introduction

RNAs play a critical role as mediators of genetic functions. Their expressions are highly dynamic and deeply intertwined with the physiological state of the whole organism (*1, 2*). However, capturing these dynamics at the scale of whole living systems remains a significant challenge in biology.

Living organisms as a whole are important for understanding RNA expression dynamics (*3*), which reflect the complex regulatory networks governing growth, development, and adaptation to environmental changes. Within individual cells, RNA expression is shaped not only by the local cellular conditions but also by systemic signals originating from distant tissues (*4, 5*). These processes are further modulated by external environmental signals that directly act on the organism as a whole. Moreover, RNAs often traffic between tissues, underscoring their dynamic nature and functional importance (*6*). Intriguingly, living organisms frequently acquire RNAs from distinct organisms that even belong to entirely different biological kingdoms (*7*). Those RNAs function within the recipients, mediating intimate interspecies relationships (*8*). Profiling such RNA dynamics across time and space at the scale of whole living organisms is crucial for understanding gene regulation and ecological interactions within interconnected biological and environmental contexts.

However, existing methods, such as fluorescence in situ hybridization (FISH) (*9*), spatial transcriptomics (*10*), aptamer-based RNA imaging (*11, 12*), and RNA-binding fluorescent proteins system such as MS2-MCP (*13*), are unable to effectively capture spatiotemporal RNA expression dynamics across the whole living organism. Recently, a split ribozyme system was introduced as an alternative for *in vivo* RNA imaging in plant (*14*). However, the delay between ribozyme-mediated reassembly of the GFP transcript and subsequent protein synthesis limits its applicability for real-time RNA tracking. To address these limitations, we developed an RNA switch-controlled RNA-triggered fluorescence system (RNA switch-RTF), enabling high-resolution visualization, monitoring, and quantification of RNA dynamics in living plants. Using RNA switch-RTF, we tracked *in vivo* expression dynamics of multiple conditionally expressed RNAs in *Arabidopsis thaliana* at subcellular and single-cell resolution throughout the entire plant. Additionally, we demonstrated the cell-to-cell trafficking of *TRANSLATIONALLY CONTROLLED TUMOR PROTEIN 1* (*TCTP1*) mRNAs (*15*) in *A. thaliana* and systematic migration of aphid long non-coding RNA *Ya1* (16) in the plant leaves. This approach provides a robust platform for studying

RNA localization and movement *in vivo*, offering critical insights into RNA function in plant physiology and ecological interactions.

Results

de novo design of RNA-triggered fluorescence (RTF) reporter system

We sought to develop a fluorescent reporter system to visualize specific RNA molecules in plants. In this system, GFP fluorescence would be detectable under specific illumination only when the target RNA is present. This requires GFP to be constitutively degraded in plants, with degradation inhibited by the presence of the target RNA (Fig.1A). Theoretically, constitutive GFP degradation can be achieved by tagging it with degron sequences, which are minimal motifs that recruit 26S proteasomes to targeted proteins (*17*).

Therefore, we first identified degrons in *Nicotiana benthamiana* leaves. By comparative proteomics, 17 proteins were abundantly accumulated only in the leaves treated with MG132, a proteasome inhibitor, compared to those treated with a mock solution (Table S1, Fig. S1, A to C). We fused 20 amino acids at the C-terminus of those proteins to the C-terminus of the GFP protein and tested their ability to promote GFP degradation (Fig. S1, D and E). 20 aa at the C terminus of Niben261Chr17g0072018 significantly enhanced GFP degradation (Fig.1B, Fig. S1E). Further analysis identified the last 4-aa of Niben261Chr17g0072018, RRRG, as degron capable of efficiently mediating GFP degradation (Fig.1B, Fig. S1F).

The RRRG degron, fused to the C terminal of six known RNA-binding peptides (RBP) (*18-23*) (Table S2), did not affect the RNA binding ability of those RBPs (Fig.1C, Fig. S1G). To assess the functionality of the RBP fused with RRRG, we next tested the abundance of GFP tagged with RBP-RRRG in the presence and absence of specific RNA aptamers. Among the six tested RBPs, GFP-BTat-RRRG and GFP-Rev-RRRG accumulated in *N. benthamiana* leaves when exposed to the specific RNA aptamers, Pepper and RRE, respectively (Fig. 1D, Fig. S1H). Notably, GFP-Rev-RRRG exhibited superior performance, displaying a strong GFP signal in the presence of RRE, while no significant signal was observed in its absence revealed by fluorescence image (Fig. 1E) and western blotting (Fig. S1, H and I).

Thus, we successfully developed the RNA-triggered fluorescence (RTF) system by manipulating GFP degradation to visualize the presence of the specific RNA ligand in plants.

Engineering of RNA switches to control GFP degradation in the RTF system

The RNA aptamer RRE binds to Rev and inhibits the recruitment of the proteasomes to the degron on the GFP-Rev-RRRG. Building on this mechanism, we started to engineer RNA switches

capable of controlling GFP degradation in the presence of specific target RNA molecules. To achieve this, we constructed RNA switches based on RRE (39 nt), incorporating three functional elements: a probe sequence to the target RNA and two linker sequences that hybridize with the RRE and the probe, respectively (Fig.1F).

Theoretically, in the absence of the target RNA, the RNA switch adopts an inactive conformation where the linkers hybridize with the RRE and the probe. This folding prevents RRE from binding to the degron, leading to GFP degradation (Fig.1G). Conversely, when the target RNA is present, the RNA switch transitions to an active conformation through base pairing between the probe and the target RNA. This conformational change allows RRE to bind to the degron, leading to GFP accumulation (Fig.1G).

To evaluate the functionality of the RNA switch, we designed various combinations of probes and linker sequences, and tested their ability to regulate GFP levels in the presence and absence of the target RNA. Using the *N. benthamiana* mCherry overexpression (OE) lines, we designed 12 distinct probes to target different regions of mCherry mRNA (Fig. S2A, Table S3). The RNA switch plasmid and the GFP-Rev-RRRG plasmid in *Agrobacterium tumefaciens* were co-infiltrated into *N. benthamiana* leaves of both mCherry OE lines and wild-type (WT) plants. Out of the 12 probes tested, probes 2 and 8 demonstrated significant functionality (Fig. S2, B and C). In WT plants, these two probes effectively maintained the RNA switch in an inactive state, as evidenced by the absence of GFP signals (Fig.1H). In mCherry OE plants, however, these probes enabled the RNA switch to bind the degron, resulting in strong GFP signals (Fig.1H).

Interestingly, RNA switches with probes 2 and 8 adopted a dumbbell-shaped structure (Fig. S2A), which appeared critical for their functionality. The RNA switch incorporated with probe 2 exhibited a shorter stem sequence and a larger bottom loop, enhancing its efficiency. Other structural configurations failed to regulate GFP signals effectively (Fig. S2, A to C), underscoring the importance of the dumbbell-shaped conformation for RNA switch performance.

Altogether, we engineered RNA switches that effectively control the RTF system, enabling precise regulation of GFP degradation in response to specific RNA molecules.

Optimization of RNA switch-controlled RTF system in plants

To evaluate the RNA switch-RTF system in plants, we constructed a plasmid containing sequences of an RNA switch targeting *CM3* mRNA driven by the U6 promoter and GFP-Rev-

RRRG under the control of the pUBQ10 promoter (Fig. 2A). These expression modules were introduced into both *A. thaliana* wild-type (WT) and *cm3* mutant plants (Fig. 2A). In WT plants, strong GFP signals were observed, but mutant plants also exhibited weak GFP signals (Fig. 2B), indicating that the system displayed some degree of signal leakage. The leakage was also confirmed by the observation of GFP in WT plants expressing the RNA switch-RTF system that were treated with an RNA synthesis inhibitor (Fig. S3, A and B).

To address this issue, we incorporated two advanced strategies: the split fluorescent protein (SFP) approach (*24*) and the SunTag system (*25*) (Fig. 2C). In the SFP strategy, GFP-Rev-RRRG was replaced with two modules: GFP_{1-10} and 24×GFP_{11}-Rev. In the SunTag strategy, GFP-Rev-RRRG was also replaced with two components: full-length GFP fused to a single-chain antibody (scFv) tagged with RRRG degron and 24×GCN4 tagged with Rev at its N-terminus. These improved RTF systems, combined with RNA switches targeting *CM3* mRNA, were introduced into WT and *cm3* mutant plants. Among the modified systems, the RTF-SunTag system exhibited an extremely low GFP signal in *cm3* mutant plants compared to the RTF and RTF-SFP systems (Fig. 2, D and E, Fig. S3C), likely due to the efficient degradation of unbound GFP.

To assess the accuracy of the RNA switch-RTF-SunTag system, we compared the localization of *CM3* mRNA indicated by the RTF-SunTag with that determined by smFISH using a series of Cy3-labeled probes targeting *CM3* mRNA. Colocalization of GFP and Cy3 signals was observed in the leaves and roots of transgenic plants engineered with the RNA switch-RTF-SunTag system (Fig. 2, F to G, Fig. S3, E and F), confirming its accuracy in detecting *CM3* mRNA localization.

In summary, the RNA switch-RTF system, optimized with the SunTag strategy and hereafter referred to as RNA switch-RTFst, accurately localizes the target RNA within plant cells, providing a robust and reliable tool for studying RNA dynamics and subcellular localization.

RNA subcellular localization is unaffected by RNA switch-RTFst system

RNA function is often closely tied to subcellular localization. We designed three experiments to assess whether the RNA switch-RTFst system influences RNA localization.

In the first experiment, we compared the subcellular localization of *CM3* mRNA resulting from the RNA switch-RTFst system with those from the mCherry-MCP-MS2 system. In the mCherry-MCP-MS2 system, repeated MS2 sequences were fused to the 3'UTR of *CM3* mRNA,

allowing the MS loops on the hybrid RNA to capture MCP from the mCherry-MCP protein (Fig. 3A). This approach revealed that *CM3* mRNAs localized in both the nuclei and cytoplasm (Fig. 3A). For the RNA switch-RTFst system, specific probe sequences targeting the 5'UTR, CDS, and 3'UTR of *CM3* mRNA were designed (Table S5). Probes targeting the CDS showed identical subcellular localization patterns to those observed with the mCherry-MCP-MS2 system (Fig. 3A, Fig. S3, G and H). Importantly, probes targeting the 5'UTR should be used with caution, as they tend to detect fewer RNA molecules per cell.

In the second experiment, the RNA switch-controlled RTFst system with a probe targeting *CM3*, and *CM3-6×MS2* RNA was co-expressed in protoplast cells of *N. benthamiana* leaves. GFP signals revealed that *CM3-6×MS2* RNA was predominantly localized in the cytoplasm and was nearly undetectable at the cytomembrane (Fig. 3, B and C). However, when MCP tagged with CAAX (membrane targeting motif) (*26*) was introduced, the GFP signal along the membrane significantly increased (Fig. 3, B and C). This change was attributed to the binding of MS loops *on CM3-6×MS2* RNA to MCP proteins at the membrane. These results suggest that the localization of *CM3-6×MS2* RNA, even when complexed with the RNA switch-RTFst, remained unaffected.

In the third experiment, we tested RNA switch-RTFst targeting the mitochondria-localized RNA *VDAC3* (*Voltage-dependent anion channels*) *(27)*. The RNA switch-RTFst system and *VDAC3* RNA were co-expressed in *N. benthamiana* leaves. Over time, the GFP signal became increasingly proximal to mitochondria (Fig. 3, D and E). This progressive colocalization suggested that *VDAC3* RNA was unaffected by the system and remained associated with its expected subcellular compartment, the mitochondria.

In summary, the RNA switch-RTFst system does not alter the subcellular localization of RNA in plants, maintaining the native localization patterns of target RNAs.

Real-time monitoring of RNA expression dynamics in living plants

With the robust RNA switch-RTFst system, we aimed to monitor the RNA expression dynamics in real time within living plants. To assess the robustness of the system, we selected RNAs representing diverse scenarios: *TUB5* (*Tubulin β-5*) for development-dependent expression *(28)*, *SMB* (*Sombrero*) for tissue-specific expression (*29*), *CCA1* (*Circadian clock associated 1*) for circadian regulation (*30*), and *CIPK11* (*CBL-interacting protein kinase 11*) for stress responsiveness, particularly to cadmium (Cd) (*31)* (Table S6). RNA switches targeting the CDS

regions of those RNAs were genetically introduced, along with the RTFst system, into *A. thaliana* wildtype plants.

TUB5 mRNA is ubiquitously expressed in *A. thaliana*, with lower levels in vegetative tissues and higher levels in stems and reproductive tissues. Fluorescence imaging revealed that GFP signals across all examined tissues of transgenic plants (Fig. 4, A and B). During the development, signals remained relatively stable in the roots but became stronger in the flowers (Fig. 4, A and B, Fig. S4, A and B). Notably, the RNA switch-RTFst system in plants showed no significant effect on the expression, turnover, or translation of *TUB5* mRNA or on the overall ubiquitinate patterns of plant proteins (Fig. S5 A to E).

SMB was exclusively expressed in the specialized zones of roots during the development. *SMB* was mainly expressed in the elongation zone of roots in the 3- and 5-day-old seedlings, with a gradual increase in expression observed in the maturation zone of the 7-day-old seedlings (Fig. 4C, Fig. S4, C and D). *CCA1* is a circadian-regulated RNA that exhibits time-of-day specific expression patterns. Its abundance displayed dynamic changes during the morning and evening phases, reflecting its circadian-dependent regulation (Fig. 4D, Fig. S4, E to F). *CIPK11*, a Cd-responsive mRNA, showed increased abundance in roots 12 hours after Cd treatment, followed by a gradual decrease at 18 hours (Fig. 4D, Fig. S4, H to I). These dynamic expressions revealed by the RNA switch-RTFst system were further validated through qRT-PCR analysis (Fig. 4, E and F, Fig. S4, G and J).

Altogether, the RNA switch-RTFst system provides a powerful tool to visualize and monitor the *in vivo* dynamics of RNA expression in living plants, offering insights into development, tissue specificity, circadian regulation, and stress responses.

Trafficking the movement of mobile RNAs in living plants

In plants, transcripts can move to distant tissues, potentially acting as systemic signals regulating development and growth. *TCTP1* mRNA exhibits long-distance mobility, traveling from the shoot to the root through the phloem (*15*). To track this movement, we expressed the *TCTP1*-targeted RNA switch-RTFst system in *tctp1* mutants (*tctp1-RTFst*) (Fig. 5A). Grafting experiments were then conducted using the wild-type plant shoots as scion and the *tctp1-RTFst* roots as stock (Fig. 5A). 72 hours post-grafting, GFP signals progressively intensified, particularly at 5 mm below the graft junction (Fig. 5, B and C). Over time, stronger GFP signals also

accumulated in root sections further from the junction (Fig. 5, B and C). Time-lapse imaging confirmed the movement of *TCTP1* mRNA across the graft junction (Fig. 5, B and D, Movie 1). Upon reaching the root, *TCTP1* mRNA is known to influence lateral root formation and regulate root architecture (*32*). Root length in grafted plants was comparable to that of WT and significantly longer than in *tctp1* mutants (Fig. 5D), suggesting that WT-derived *TCTP1* mRNA effectively compensated for the loss of function in the roots. Notably, this compensation was unaffected by the RNA switch-RTFst in the roots.

Visualization of aphid-secreted lncRNA *Ya1* in plants

Beyond endogenous RNA movement within plants, RNAs can also be transferred between organisms even belonging to distinct biological backgrounds. Previously, we discovered that *Myzus pericase* (green peach aphid, GPA) translocate the lncRNA *Ya1* into the host plants via feeding (*16*). To investigate the mobility of this aphid- secreted RNA, we designed a *Ya1*-targeted RNA switch-RTFst and expressed it in *N. benthamiana* leaves via agroinfiltration. When co-expressed with *Ya1*, GFP signals were detected in the cytoplasm and nuclei of infiltrated cells (Fig. 6A). In leaves where the system was expressed and subsequently fed on by GPA, GFP signals accumulated at the feeding sites (Fig. 6A). Furthermore, when the system was expressed in two separate infiltration sites on the same leaf, one co-expressing *Ya1*, GFP signals were observed at the distal site, even in the absence of direct *Ya1* expression (Fig. 6B, Movie 2). To visualize the dynamic of *Ya1* translocation, *N. benthamian* leaves expressing *Ya1*-targeted RNA switch-RTFst were subjected to GPA feeding and were monitored by time-lapse imaging. After six hours of continuous feeding, GFP signal was detectable and intensified over time, while the control leaves expressing the system but without aphid feeding exhibited no detectable GFP signal (Fig. 6C).

These findings provide direct evidence of the mobility of an aphid- secreted cross-kingdom RNA in the host plant.

Discussions

Monitoring RNA expression dynamics in living systems at the whole-organism scale remains a fundamental challenge in biology. Here, we have addressed this issue by introducing the RNA switch-RTF system, *de novo* designed platform for visualizing RNA expression dynamics in living

plants. This system enables high-sensitivity detection of target RNAs while preserving their native localization and function.

Over the past several decades, live-cell RNA imaging technologies have become indispensable for quantitatively analyzing RNA expression dynamics (*33*). However, those methods face significant limitations that hinder their ability to monitor real-time RNA dynamics at the whole-organism scale. Nucleic acid molecular beacons (*34*) and nanoparticle-based "nano-flares" (*35*) produce fluorescence upon structural reconfiguration triggered by RNA binding. However, efficient delivery of these exogenously synthesized probes into plant cells remains a major challenge due to the barrier of plant cell walls (*24*). Fluorescent RNA aptamers and RNA motifs that recruit RNA-binding fluorescent proteins offer another strategy for RNA visualization (*36-38*), but require tissue separation, which disrupts the native RNA Expression patterns and compromises spatial regulatory information. CRISPR/dCas-based imaging enables visualization of diverse RNAs and their subcellular localization (*39*), yet its application in plant cells is confounded by cytosolic fluorescence artifacts (*40*). Recently, a split ribozyme system was introduced as an alternative for *in vivo* RNA imaging in plants (*14*). This approach disrupts sfGFP translation by incorporating a self-splicing ribozyme into its coding sequence, allowing translation to proceed only after the ribozyme excises and transcript ligation (*14*). While promising when target RNA and sfGFP translation occur in the same cell, the temporal delay between transcript rejoining and protein synthesis constrains its utility for real-time RNA tracking.

The effectiveness of the RNA switch-RTF system relies on the precise design of RNA-triggered fluorescence (RTF) and programmable RNA switches. A critical component of the RTF is the degron RRRG, which drives the continuous GFP degradation. While several degrons have been identified in plants, including the Auxin-inducible degron (AID) (*41*) and mini-Auxin inducible degron (mIAA) (*42*), their lengths, ranging from 67 to 110 amino acids for AID and 40 to 50 amino acids for mIAA, render them unsuitable for development into RNA-binding peptides. To overcome this limitation, we conducted a proteome-wide screening of constitutively degraded proteins in plants, leading to the identification of RRRG, a 4-amino acid degron located at the C-terminus of Niben261Chr17g0072018. This represents the smallest degron identified in plants to date. Importantly, RRRG did not disrupt the RNA binding activity of known RNA-binding proteins (RBPs) or their interaction with specific RNA ligands.

The second key component of the system is the RNA switch, which regulates the degradation of GFP-RRRG. Leveraging the high affinity between Rev-RRRG and the RNA aptamer RRE (*22*), we engineered RNA switches by incorporating probe and linker sequences into RRE. Systematic testing of probe-linker combinations led to the identification of dumbbell-shaped RNA switches capable of modulating GFP degradation in response to specific RNAs. This regulation is mediated by RNA allostery, wherein binding to target RNAs induces conformational changes that alter the ability of RRE to interact with the degron on GFP-RRRG. These RNA switches represent the first successfully engineered RNA-based regulatory elements in plants, demonstrating robust functionality across transient expression systems, including protoplasts and agroinfiltrated leaves, as well as in stable transgenic lines.

Integration of the RNA switch-RTF system with the SunTag strategy markedly enhances the sensitivity and precision of RNA detection. Crucially, the RNA switch-RTFst complex does not perturb the localization, expression, turnover, or translation of target RNA molecules. It also preserves target RNA function, as demonstrated by the successful compensation of shoot-derived *TCTP1* mRNA in the root tissues of *tctp1* mutants expressing the RNA switch-RTFst complex. Beyond its utility in tracking RNA dynamics in living plants, the RNA switch-RTF system holds promise in RNA-triggered immune responses. By engineering the system to detect pest-secreted RNAs (*43*, *44*), it could be repurposed to trigger the accumulation of pest-specific defense molecules instead of GFP. Similarly, many plant pathogens secrete RNAs into host cells even at early infection stages (*45-47*). The RNA switch-RTF system can be designed to recognize these pathogen-derived RNAs and activate species-specific immune responses.

These findings establish the RNA switch-RTF system as a versatile platform for RNA imaging and functional studies while opening new avenues for enhancing plant immunity against pests and pathogens.

References

1. S. Hani *et al.*, Live single-cell transcriptional dynamics via RNA labelling during the phosphate response in plants. *Nat. Plants* **7**, 1050-1064 (2021).
2. L. López-Maury, S. Marguerat, J. Bähler, Tuning gene expression to changing environments: from rapid responses to evolutionary adaptation. *Nat. Rev. Genet.* **9**, 583-593 (2008).
3. S. Alamos, A. Reimer, K. K. Niyogi, H. G. Garcia, Quantitative imaging of RNA polymerase II activity in plants reveals the single-cell basis of tissue-wide transcriptional dynamics. *Nat. Plants* **7**, 1037-1049 (2021).
4. L. Liu, X. Chen, Intercellular and systemic trafficking of RNAs in plants. *Nat. Plants* **4**, 869-878 (2018).
5. L. Corbesier *et al.*, FT protein movement contributes to long-distance signaling in floral induction of Arabidopsis. *Science* **316**, 1030-1033 (2007).
6. C. J. Thieme *et al.*, Endogenous messenger RNAs transported to distant tissues. *Nat. Plants* **2**, 15025-15032 (2016).
7. J. H. Westwood, G. Kim, RNA mobility in parasitic plant - host interactions. *RNA Biol.* **14**, 450-455 (2017).
8. M. Wang, N. Thomas, H. Jin, Cross-kingdom RNA trafficking and environmental RNAi for powerful innovative pre- and post-harvest plant protection. *Curr. Opin. Plant Biol.* **38**, 133-141 (2017).
9. A. Bleckmann, T. Dresselhaus, Fluorescent whole-mount RNA in situ hybridization (F-WISH) in plant germ cells and the fertilized ovule. *Methods* **98**, 66-73 (2016).
10. M. T. Islam *et al.*, Advances in the Application of Single-Cell Transcriptomics in Plant Systems and Synthetic Biology. *Biodes. Res.* **6**, 1-17 (2024).
11. J. Bai *et al.*, A protein-independent fluorescent RNA aptamer reporter system for plant genetic engineering. *Nat. commun.* **11**, 3847 (2020).
12. X. J. Chen *et al.*, Visualizing RNA dynamics in live cells with bright and stable fluorescent RNAs. *Nat. Biotechnol.* **37**, 1287-1293 (2019).
13. D. Fusco *et al.*, Single mRNA molecules demonstrate probabilistic movement in living mammalian cells. *Curr. Biol.* **13**, 161-167 (2003).
14. Y. Liu *et al.*, A split ribozyme system for in vivo plant RNA imaging and genetic engineering. *Plant Biotechnol. J.* **1**, 1-10 (2025).
15. L. Yang *et al.*, m^5C Methylation Guides Systemic Transport of Messenger RNA over Graft Junctions in Plants. *Curr. Biol.* **29**, 2465-2476 (2019).
16. Y. Z. Chen *et al.*, An aphid RNA transcript migrates systemically within and is a virulence factor. *P. Natl. Acad. Sci. USA* **117**, 12763-12771 (2020).
17. X. Y. Chen *et al.*, Molecular basis for arginine C-terminal degron recognition by $Cul2^{FEM1}$ E3 ligase. *Nat. Chem. Biol.* **17**, 1552-4450 (2021).
18. R. J. Austin, T. Xia, J. Ren, T. T. Takahashi, R. W. Roberts, Designed arginine-rich RNA-binding peptides with picomolar affinity. *J. Am. Chem. Soc.*, 10966-10967 (2002).
19. C. A. Smith, V. Calabro, A. D. Frankel, An RNA-Binding Chameleon. *Mol. Cell* **6**, 1067-1076 (2000).
20. F. Jiang *et al.*, Anchoring an extended HTLV-1 Rex peptide within an RNA major groove containing junctional base triples. *Struct. Fold. Des.* **7**, 1461-1472 (1999).
21. P. Legault, J. Li, J. Mogridge, L. E. Kay, J. Greenblatt, NMR Structure of the Bacteriophage λ N Peptide/boxB RNA Complex: Recognition of a GNRA Fold by an Arginine-Rich Motif. *Cell* **93**, 289-299 (1998).

22. J. L. Battiste *et al.*, Alpha helix-RNA major groove recognition in an HIV-1 rev peptide-RRE RNA complex. *Science* **273**, 1547-1551 (1996).
23. J. D. Puglisi, L. Chen, S. Blanchard, A. D. Frankel, Solution Structure of a Bovine Immunodeficiency Virus Tat-TAR Peptide-RNA Complex. *Science* **270**, 1200-1203 (1995).
24. N. C. Huang, K. R. Luo, T. S. Yu, Development of a split fluorescent protein-based RNA live-cell imaging system to visualize mRNA distribution in plants. *Plant Methods* **18**, 1-10 (2022).
25. M. Chen *et al.*, Live imaging of RNA and RNA splicing in mammalian cells via the dcas13a-SunTag-BiFC system. *Biosens. Bioelectron.* **204**, 1-11 (2022).
26. A. Fischer, W. W. D. Mühlhäuser, B. Warscheid, G. Radziwill, Membrane localization of acetylated CNK1 mediates a positive feedback on RAF/ERK signaling. *Sci. Adv.* **3**, 1-10 (2017).
27. M. Michaud *et al.*, Differential targeting of VDAC3 mRNA isoforms influences mitochondria morphology. *P. Natl. Acad. Sci. USA* **111**, 8991-8996 (2014).
28. M. Bach-Pages *et al.*, Discovering the RNA-Binding Proteome of Plant Leaves with an Improved RNA Interactome Capture Method. *Biomolecules* **10**, 1-21 (2020).
29. L. L. Zheng *et al.*, A root cap-localized NAC transcription factor controls root halotropic response to salt stress in Arabidopsis. *Nat. Commun.* **15**, 1-12 (2024).
30. P. de los Reyes *et al.*, CONSTANS alters the circadian clock in Arabidopsis thaliana. *Mol. Plant* **17**, 1204-1220 (2024).
31. S. B. Gu *et al.*, The kinase CIPK11 functions as a positive regulator in cadmium stress response in Arabidopsis. *Gene* **772**, 1-9 (2021).
32. R. Branco, J. Masle, Systemic signalling through translationally controlled tumour protein controls lateral root formation in Arabidopsis. *J. Exp. Bot.* **70**, 3927-3940 (2019).
33. E. Braselmann, C. Rathbun, E. M. Richards, A. E. Palmer, Illuminating RNA Biology: Tools for Imaging RNA in Live Mammalian Cells. *Cell Chem. Biol.* **27**, 891-903 (2020).
34. J. Göhring, J. Jacak, A. Barta, Imaging of Endogenous Messenger RNA Splice Variants in Living Cells Reveals Nuclear Retention of Transcripts Inaccessible to Nonsense-Mediated Decay in Arabidopsis. *Plant Cell* **26**, 754-764 (2014).
35. A. E. Prigodich *et al.*, Nano-flares for mRNA Regulation and Detection. *ACS Nano* **3**, 2147-2152 (2009).
36. M. F. Al Mazid, O. Shkel, Y. Kharkivska, J. S. Lee, Application of fluorescent turn-on aptamers in RNA studies. *Mol. Omics* **17**, 483-491 (2021).
37. L. Truong, A. R. Ferré-D'Amaré, From fluorescent proteins to fluorogenic RNAs: Tools for imaging cellular macromolecules. *Protein Sci.* **28**, 1374-1386 (2019).
38. T. G. Pham, J. Wu, Recent advances in methods for live-cell RNA imaging. *Nanoscale* **16**, 5537-5545 (2024).
39. V. Singh, M. Jain, Recent advancements in CRISPR-Cas toolbox for imaging applications. *Crit. Rev. Biotechnol.* **42**, 508-531 (2022).
40. K. Luo, N. Huang, T. Yu, Selective Targeting of Mobile mRNAs to Plasmodesmata for Cell-to-Cell Movement. *Plant Physiol.*, 604-614 (2018).
41. A. Yesbolatova, T. Natsume, K. Hayashi, M. T. Kanemaki, Generation of conditional auxin-inducible degron (AID) cells and tight control of degron-fused proteins using the degradation inhibitor auxinole. *Methods* **164**, 73-80 (2019).
42. J. J. Sepers *et al.*, The mIAA7 degron improves auxin-mediated degradation in Caenorhabditiselegans. *G3 (Bethesda)* **12**, 1-15 (2022).
43. W. H. Han *et al.*, A small RNA effector conserved in herbivore insects suppresses host plant

defense by cross-kingdom gene silencing. *Mol. Plant* **18**, 1-20 (2025).
44. Z. L. Zhang *et al.*, Cross- kingdom RNA interference mediated by insect salivary microRNAs may suppress plant immunity. *P. Natl. Acad. Sci. USA* **121**, 1-9 (2024).
45. S. Wang *et al.*, Plant mRNAs move into a fungal pathogen via extracellular vesicles to reduce infection. *Mol. Plant Microbe In.* **37**, 29-29 (2024).
46. A. Chen *et al.*, Improving RNA-based crop protection through nanotechnology and insights from cross-kingdom RNA trafficking. *Curr. Opin. Plant. Biol.* **76**, 1-22 (2023).
47. A. Weiberg *et al.*, Fungal Small RNAs Suppress Plant Immunity by Hijacking Host RNA Interference Pathways. *Science* **342**, 118-123 (2013).

Acknowledgments

We sincerely thank Professor Yuelin Zhang (Sichuan University) for his insightful discussions and critical reading of the manuscript. We also appreciate Dr. Yiliang Ding (John Innes Centre, UK) and Dr. Xiaofei Yang (Center for Excellence in Molecular Plant Sciences, Chinese Academy of Sciences, China) for their valuable suggestions.

Funding:

National Natural Science Foundation of China (Grant Nos. 32201241 to JB)

National Natural Science Foundation of China (Grant Nos. 32171457 to YZ)

National Natural Science Foundation of China (Grant Nos. 22325406 to JL)

China Postdoctoral Science Foundation (Grant No. 2022M722280 to JB)

Hubei Hongshan Laboratory (Grant No. 2022hszd026 to YC)

Fundamental Research Funds for the Central Universities (Grant No. 2022ZKPY003 to YC)

Author contributions:

Conceptualization: JB, YZ, YC, CF

Methodology: JL, SP, YT, ML

Investigation: JB, JZ, HR

Visualization: SL, JY, MD, FC

Funding acquisition: JB, YZ, YC, JL

Project administration: YZ, CF

Supervision: YZ, CF

Writing – original draft: JB

Writing – review & editing: YC, YZ, CF

Competing interests: The authors declare no competing interests.

Data and materials availability: All data are available in the main text or the supplementary materials. All materials (seed stocks, plasmids) are available upon request.

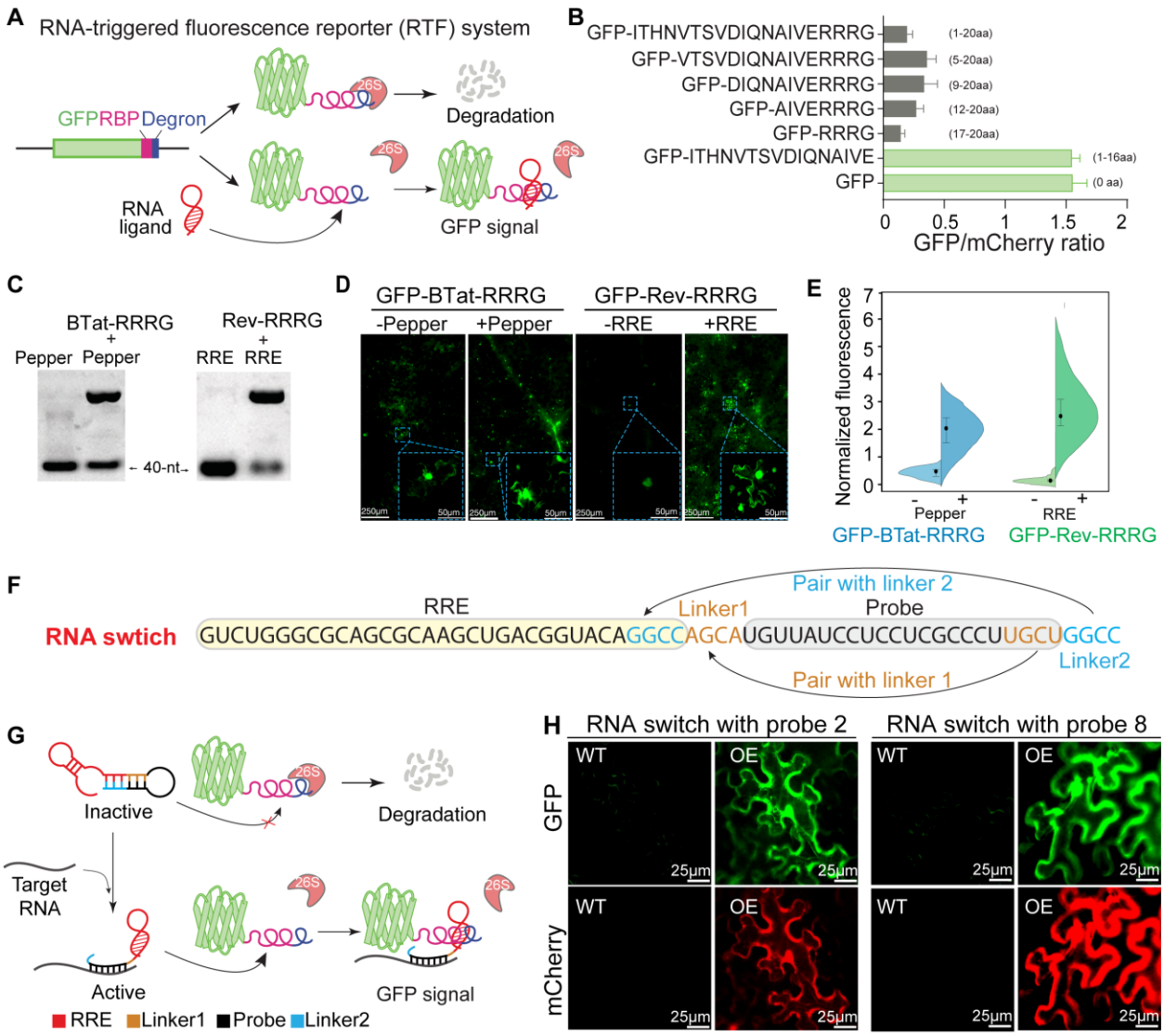

Fig.1 Design of RNA switch-controlled RTF system. **(A)** Schematic of the RTF reporter system. The fused protein GFP-RBP-Degron undergoes degradation in the absence of RNA ligands. The binding of the RNA ligand to the RBP on the fused protein blocks accessibility to the 26S proteasome, resulting in GFP signal accumulation. **(B)** Assessment of the degradation ability of putative degron sequences. Degradation efficiency was evaluated based on the GFP/mCherry fluorescence intensity ratio. mCherry and GFP tagged with the putative degron sequence were co-expressed using a 2A self-cleaving peptide system (Fig. S1A). The mCherry-2A-GFP-degron construct was cleaved at the 2A site, producing separate mCherry and GFP-degron proteins. **(C)** Binding abilities of BTat -RRRG and Rev-RRRG to their specific RNA ligands, Pepper and RRE, respectively. **(D** and **E)** GFP fluorescence signals in the absence and presence of specific RNA

ligands when tagged with BTat-RRRG or Rev-RRRG. **(F)** Design of RNA switch. Sequences shaded in yellow were the RRE, and shaded in grey were the probe. The sequences in brown were the linker 1 and those in blue were the linker 2. **(G)** Diagram of the RNA switch-controlled RTF reporter system. In the absence of the target RNA, the RNA switch adopts an inactive state through base pairing between linkers and their complementary nucleotides in the probe and RRE. When the target RNA is present, the probe hybridizes with the target, unfolding the RNA switch and enabling it to bind the RBP in GFP-RBP-RRRG. **(H)** RNA switches containing probe 2 and probe 8, which target mCherry RNA, were inactive in *N. benthamiana* WT plants but active in *N. benthamiana* mCherry overexpression (OE) lines.

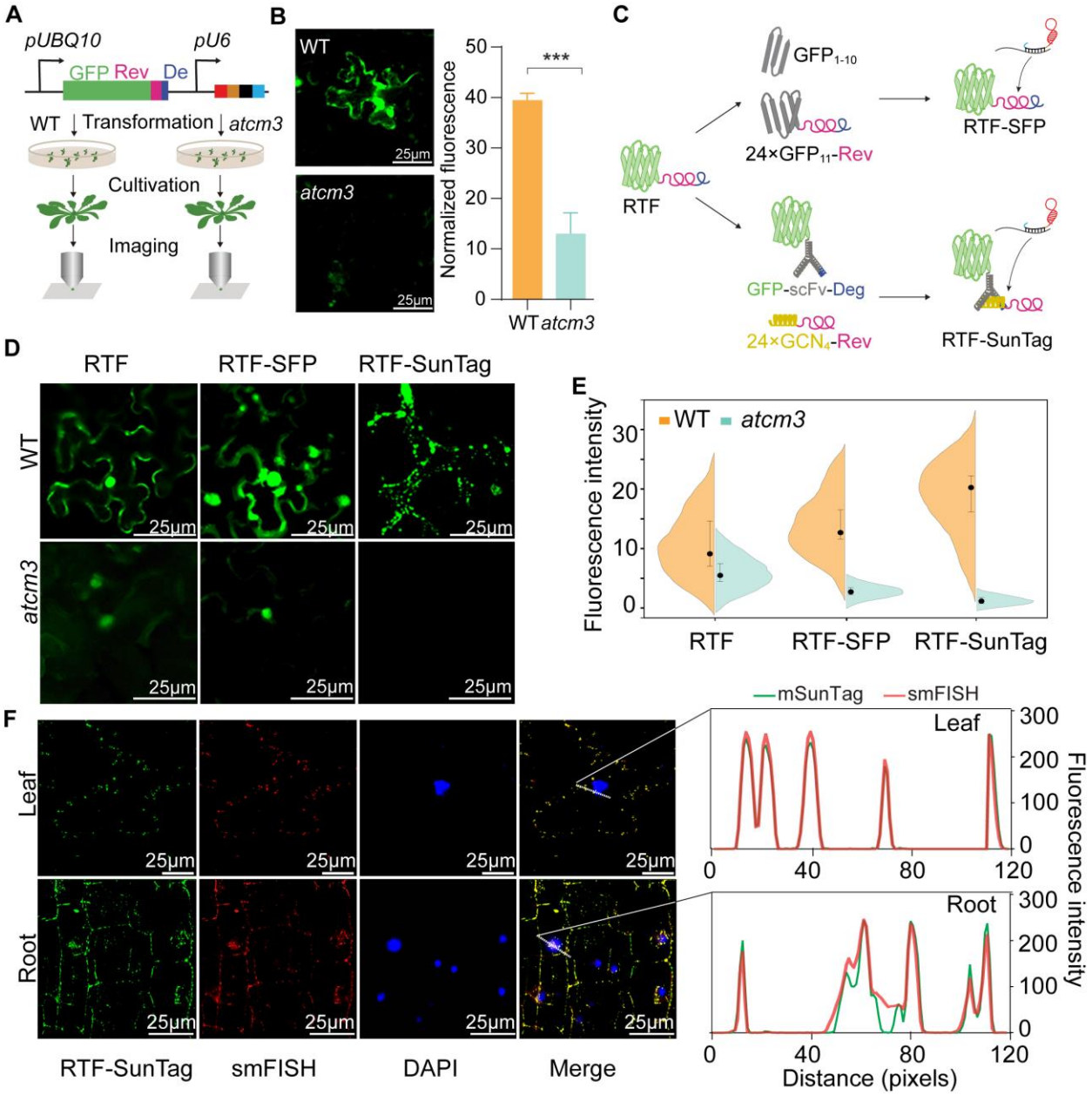

Fig. 2 Optimizing the RNA switch-RTF system in plants. **(A)** Schematic representation of introducing the RNA switch-RTF system into plants. The RTF system, driven by the pUBQ10 promoter, and the RNA switch targeting *CM3* mRNA, driven by the U6 promoter, were constructed on the same plasmid. The plasmids were introduced into *A. thaliana* WT and *cm3* mutant plants. **(B)** GFP fluorescence signals in WT and *cm3* mutant plants. **(C)** Optimizing GFP reporter by replacing with split fluorescent protein (SFP) approach and SunTag system. **(D** and **E)** Fluorescence signals in *A. thaliana* WT and *cm3* mutant plants genetically introduced with RNA switch-controlled RTF, RTF-SFP, or RTF-SunTag systems. **(F)** Localization of *CM3* mRNA

visualized using the RNA switch-RTF-SunTag system and smFISH. Cy3-labeled probes specific to *CM3* mRNA were used for smFISH. The fluorescence intensity of labeled regions in the merged images is shown on the right. Green lines represent GFP fluorescence intensity, while red lines indicate Cy3 fluorescence intensity.

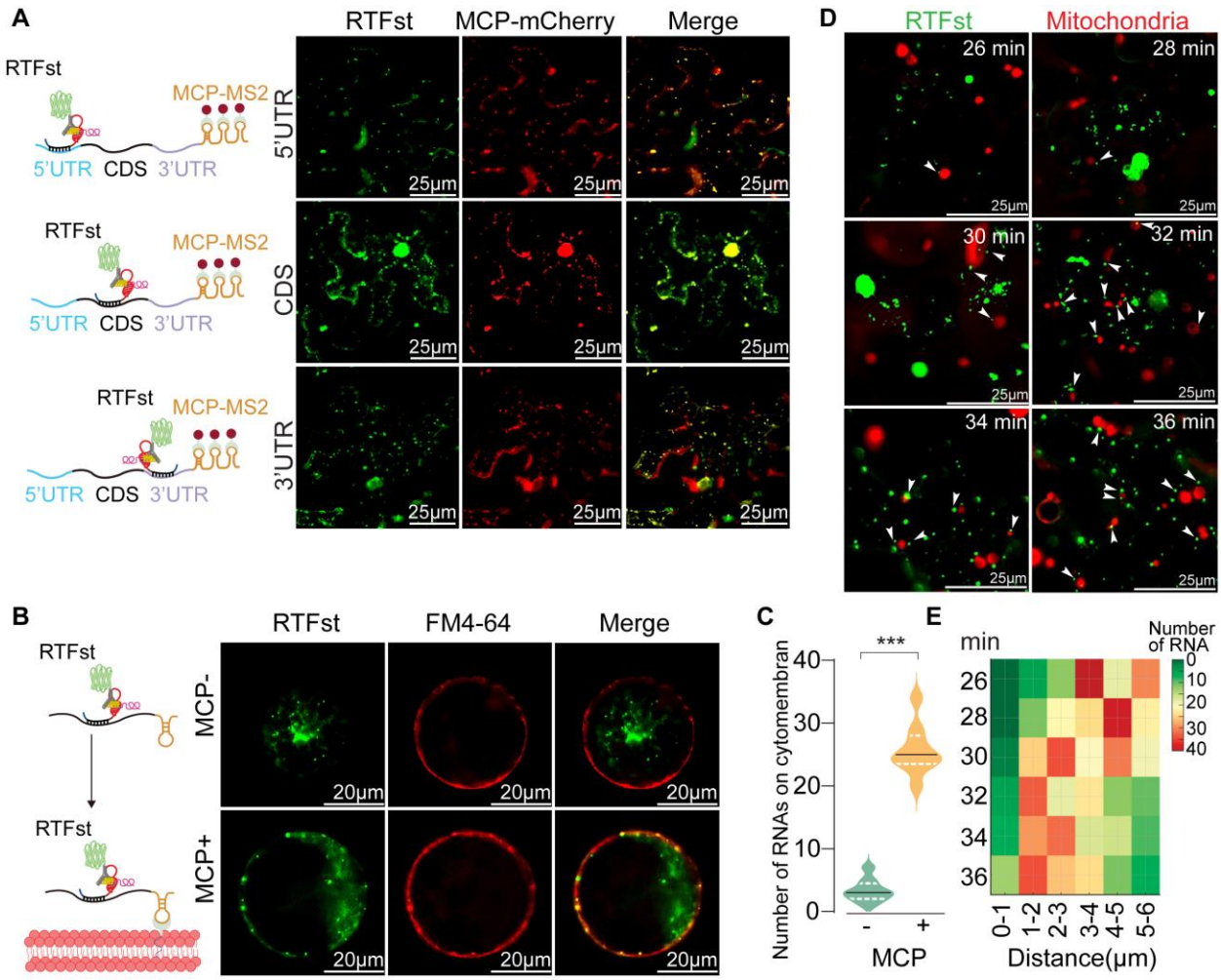

Fig. 3 RNA localization is unaffected by the RNA switch-RTFst complex. (A) RNA localization determined by the RNA switch-RTFst system is comparable to that assessed by the MCP-MS2 system. The MCP-MS2 plasmid contains 24×MS2 loops fused to sequences coding for the 5′UTR, CDS, and 3′UTR of *CM3* mRNA, driven by the pUBQ10 promoter, as well as MCP sequences driven by the CaMV35S promoter. The MCP-MS2 plasmid and the RNA switch-RTFst plasmid with probes targeting the 5′UTR, CDS, or 3′UTR were co-expressed in *N. benthamiana* WT leaves via agroinfiltration. **(B)** The RNA switch-RTFst complex targeting *CM3* mRNA did not significantly affect RNA localization. For the MCP- condition, the RNA switch-RTFst plasmid with a probe targeting the *CM3* CDS and a plasmid expressing *CM3-MS2* mRNA were co-expressed in *N. benthamiana* mesophyll protoplasts. For the MCP+ condition, the RNA switch-RTFst plasmid, and the *CM3-MS2* mRNA plasmid containing the MCP protein sequence tagged with CAAX (a membrane targeting motif) were co-expressed in *N. benthamiana* mesophyll

protoplasts. Cytomembranes were stained with FM4-64. **(C)** Quantification of RNAs localized to the cytomembrane. Statistical significance (***$p < 0.001$) was calculated using two-tailed unpaired Student's *t*-test. **(D)** *VDAC3* RNA with the RNA switch-RTFst complex localizes to mitochondria. Green dots represent *VDAC3* RNAs visualized by RNA switch-RTFst, while red dots indicate mitochondria stained with Red CMXRos. White arrows highlight *VDAC3* RNAs in proximity to mitochondria. **(E)** The number of *VDAC3* RNAs in proximity to mitochondria increased over time.

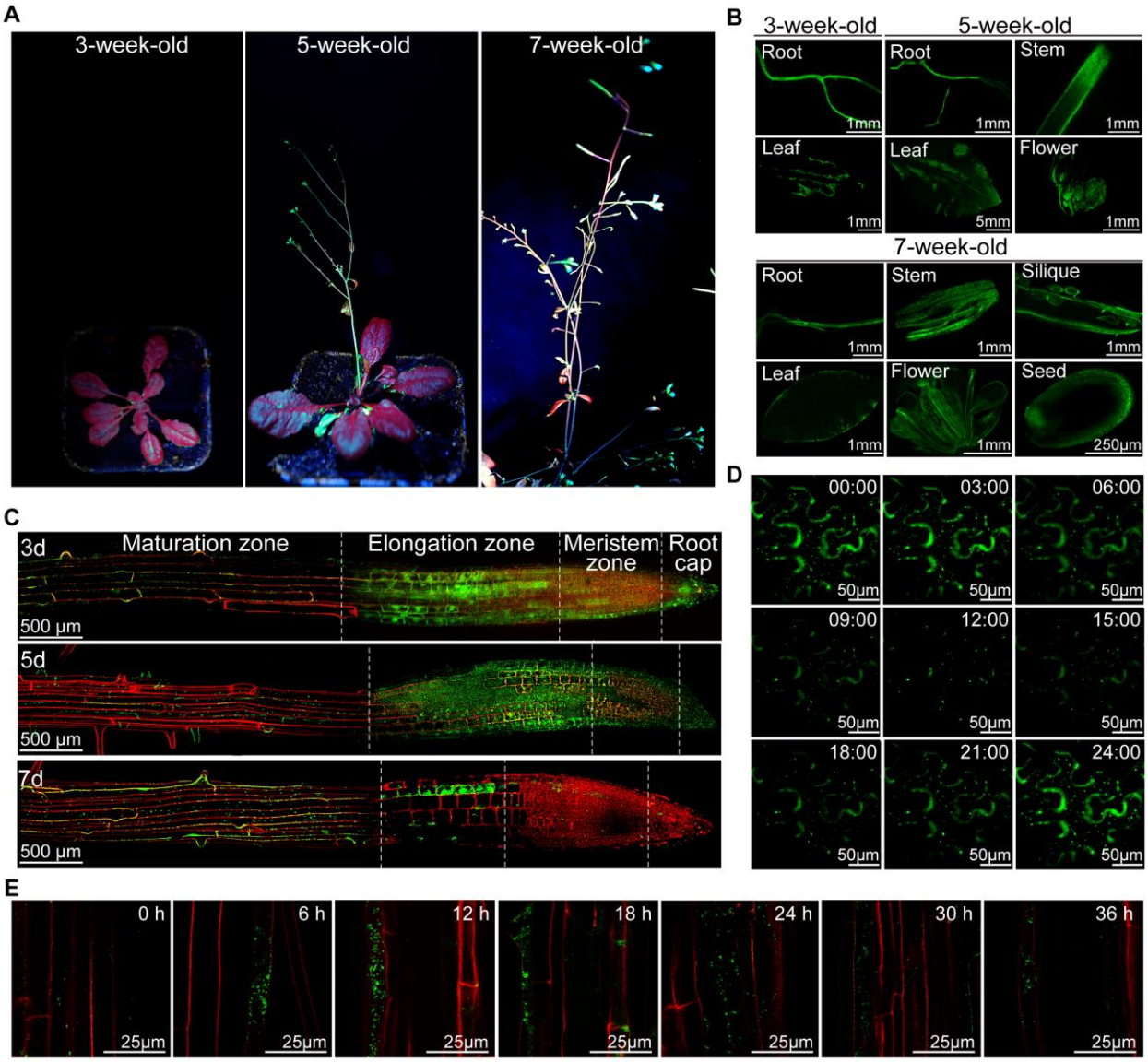

Fig. 4 Monitoring RNA expressions in living plants. (A and **B)**. Developmental stage- and tissue-dependent expression levels of *TUB5*. Transgenic *A. thaliana* plants expressing the RNA switch-RTFst targeting *TUB5* RNAs were analyzed. **(C)** Tissue-specific expression patterns of *SMB*. Root tips from transgenic *A. thaliana* plants expressing the RNA switch-RTFst targeting *SMB* RNAs were harvested. Cell walls (red) were stained with propidium iodide. **(D)** Circadian-regulated expression patterns of *CCA1*. Leaves from 7-week-old transgenic *A. thaliana* plants expressing the RNA switch-RTFst targeting *CCA1* RNAs were collected every 3 hours, and GFP signals were observed. **(E)** Cd-induced expression patterns of *CIPK11*. Seven-week-old transgenic *A. thaliana* plants expressing the RNA switch-RTFst targeting *CIPK11* RNAs were treated with 50 μM Cd. Roots were harvested every 6 hours post-treatment, and GFP signals were recorded.

Cell walls (red) were stained with propidium iodide. Green fluorescence represents target RNAs visualized by the RNA switch-RTFst.

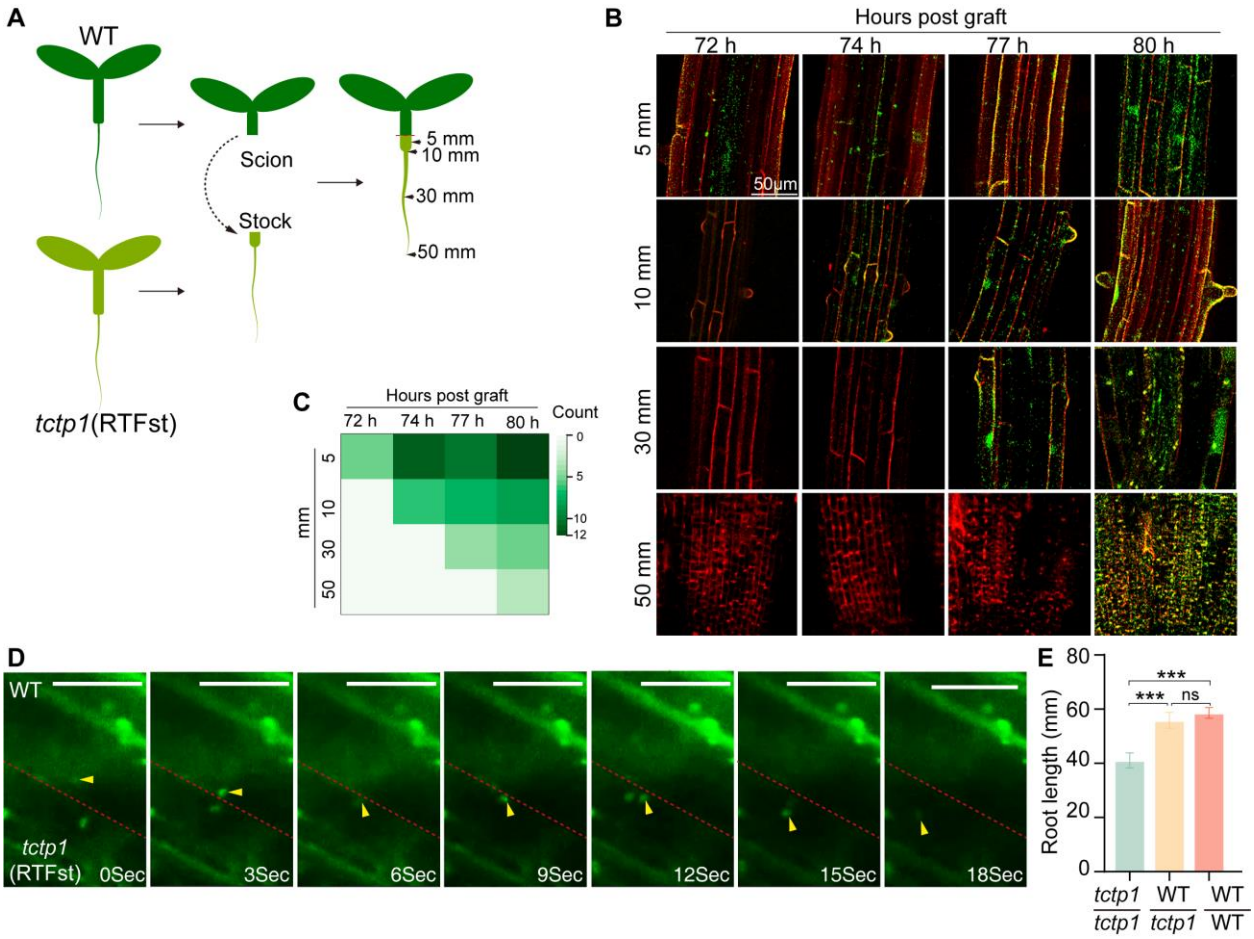

Fig. 5 Trafficking cell-to-cell movement of *TCTP1* RNA. (A) Schematic view of hypocotyl grafting. One-week-old Arabidopsis seedlings of similar size and with evenly elongated hypocotyls were cut in the upper half of the hypocotyl with a sterilized razor blade. The WT shoots were used as scions and *tctp1-RTFst* roots as stocks. The red dash line indicates the grafting junctions. The black arrowhead indicates the positions of 5 mm, 10 mm, 15 mm, and 20 mm below the graft junctions. Grafted plants were grown vertically under short-day conditions. **(B)** Representative imaging of *TCTP1* RNA in different positions of grafted seedlings post grafting. Cell walls (red) were stained with propidium iodide. **(C)** The number of grafted plants exhibiting fluorescence signals at various times post-grafting. A total of 12 grafted seedlings were imaged for each selected position below the graft junction. **(D)** Real-time fluorescence imaging of cell-to-cell movement of *TCTP1* RNA in root cells of grafted plants. See **Movie 1** for details. The red dashed line indicates the cell boundary, and the yellow arrowhead indicates *TCTP1* RNA. The scale bar was 25 μm. (**E**)**.** Root length of tctp1 mutants, grafted plants, WT plants (n = 6, mean ± s.e.m., *** $P < 0.001$, two-tailed unpaired Student's t-test).

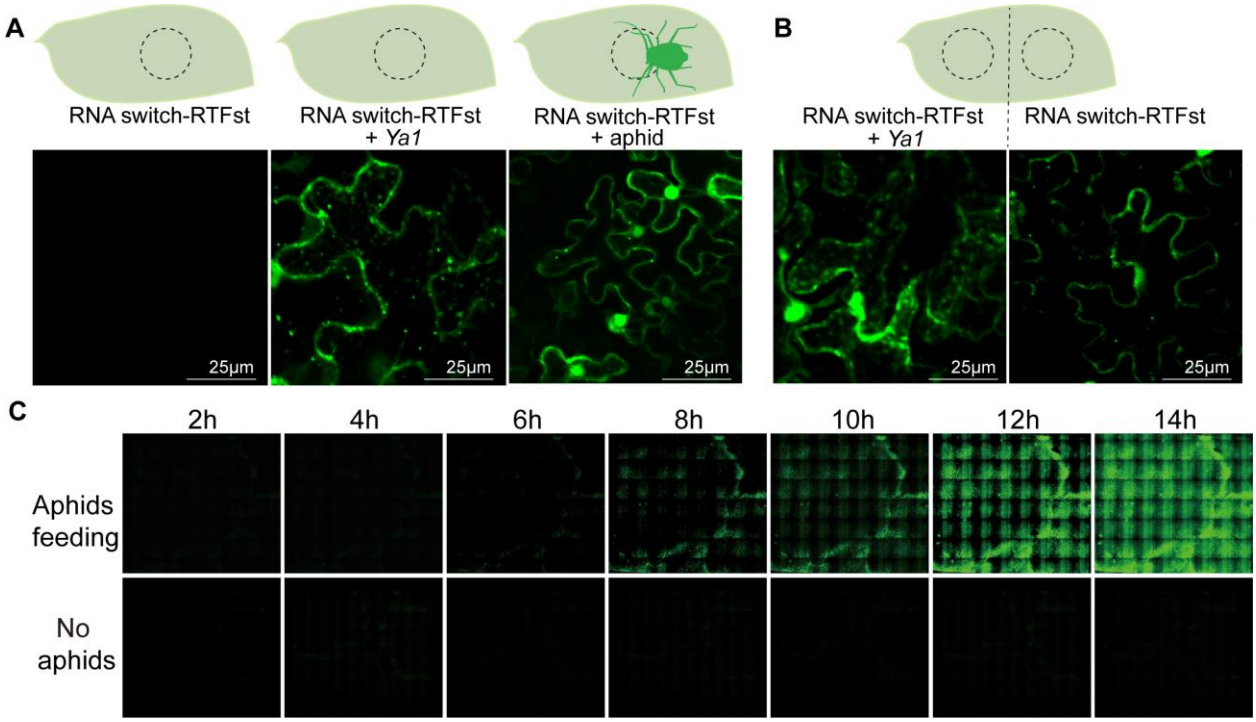

Fig. 6 Visualization of aphid-secreted lncRNA *Ya1* in the *N. benthamiana* leaves. (A) Subcellular localization of *Ya1*. RNA switch-RTFst+*Ya1*, RNA switch-RTFst and *Ya1* were co-expressed via agroinfiltration. RNA switch-RTFst+aphid, GPA fed on the *N. benthamiana* leaves that RNA switch-RTFst was expressed. **(B)** *Ya1* was visualized at the distal site. **(C)** Real-time fluorescence imaging of aphid-secreted *Ya1* in the leaves. See **Movie 2** for details.

Supplementary Material

RNA-triggered fluorescence controlled by RNA switches for real-time RNA expression tracking in living plants

Jiuyuan Bai[1,2]†, Yazhou Chen[3,4]†, Jiayu Zhang[1], Jiang Li[5], Hongpei Ren[1], Yiran Tao[1], Shan Pan[1], Miaomiao Lei[1], Mengyue Dong[1]， Jia Yi[1], Sha Liu[1], Fang Chen[1], Chunhai Fan[6]*, Yun Zhao[1]*

†J.B. and Y.C. contributed equally to this work.

*Corresponding author. Email: fanchunhai@sjtu.edu.cn; zhaoyun@scu.edu.cn

The PDF file includes:

Materials and Methods

Figs. S1 to S5

Tables S1 to S10

References

Other Supplementary Materials for this manuscript include the following:

Movies S1

Movies S2

Materials and Methods

Plant materials and growth conditions

N. benthamiana and *A. thaliana* plants were grown in the soil pots in a greenhouse under a 16-hour light/8-hour dark cycle at 22 °C. The *A. thaliana* mutants *cm3* (SALK_011276.36.40.x) *and attctp1* (CS486456, heterozygous) were obtained from the Arabidopsis Biological Resource Center (ABRC). Homozygous plants were used. Primers for genotyping were listed in Table S7.

Agroinfiltration of *N. benthamiana*

Agrobacterium stocks were streaked on LB plates supplemented with kanamycin (50 μg/mL) and rifampicin (25 μg/mL). After overnight culture in liquid LB, cells were pelleted, resuspended in infiltration medium (10 mM MES, pH 5.6; 10 mM $MgCl_2$; 150 μM acetosyringone), and adjusted to an OD600 of ~0.6. After a 2-hour incubation, the suspension was infiltrated into the abaxial side of 3-week-old *N. benthamiana* leaves using a needleless syringe. Co-infiltration used a 1:1 volume ratio of bacterial solutions. Plants were maintained in growth chambers for 3 days before leaf samples were collected for confocal microscopy.

Identification of putative degrons in *N. benthamiana*

The leaves of 6-week-old *N. benthamiana* were treated with either 10 μM MG132 or mock solution (1×PBS buffer) for 24 hours, respectively. Following the treatment, leaves were harvested for LC-MS/MS at Shanghai Personalbio Technology Company. Leaf tissues were frozen, grounded, and treated with TCA/Acetone buffer and SDT buffer (4%SDS, 100mM Tris-HCl, pH7.6). The mixture was sonicated, boiled, and centrifuged to separate the supernatant. Protein concentration was determined using the BCA Protein Assay Kit (Cat. A65453, Thermo Scientific), and 15 μg of protein from each sample was mixed with 5×loading buffer and boiled. The proteins were separated on a 4%-20% SDS-PAGE gel and visualized with Coomassie Blue R-250 staining. Protein digestion was performed by adding DTT (40 mM) to each sample, mixing at 600 rpm for 1.5 h (37℃), and then adding IAA (20 mM) to block reduced cysteine residues. The samples were then transferred to filters (Microcon units, 10 kDa), washed with UA buffer (8 M urea, 100 Mm Tris-HCl pH 8.0) and 25 NH_4HCO_3 buffer, then trypsin was added (trypsin: protein (wt/wt) ratio was 1:50) and incubated at 37℃ for 15-18 h. The resulting peptides were collected, desalted on C18 Cartridges (Cat.66871-U, Sigma), concentrated by vacuum centrifugation, and reconstituted in 0.1% formic acid. For the analysis of Data independent acquisition (DIA) experiments, iRT (indexed retention time) calibration peptides were spiked into the sample and analyzed by an

OrbitrapTM AstralTM mass spectrometer connected to a Vanquish Neo system liquid chromatography in DIA mode. The precursor ions were scanned at a mass range of 380-980m/z, and the MS1 resolution was 240000 at 200 m/z. DIA data was analyzed with DIA-NN software (*1*), and protein identification was based on 99% confidence and a false discovery rate ≤ 1%. Proteins were identified by searching MS/MS against the InterPro member database Pfam.

To evaluate the degradation efficiency of putative degron sequences, the 60 nucleotides (corresponding to 20 amino acids) for each gene were cloned to the C terminus of the GFP sequence in a 2A self-cleaving peptide co-expression plasmid (Table S1). This plasmid also co-expresses mCherry alongside the fused GFP. Various truncated versions of CP6031.1(Niben261Chr17g0072018) were generated and inserted into the plasmid. These plasmids were introduced to *N. benthamiana* leaves via agroinfiltration. Degradation efficiency was assessed by comparing the GFP signal intensity to that of mCherry. The fluorescence images were captured using a confocal microscope.

Synthesize of RNA-binding peptides, RNA aptamers, and electrophoretic mobility shift assay

The RNA-binding peptides (Rev-RRRG, P22N-RRRG, λN-RRRG, BTat-RRRG, HTat-RRRG, and Rex-RRRG, Table S2) were synthesized using standard Fmoc solid-phase synthesis at Sangon Biotechnology company. Briefly, the synthesis of peptides was carried out on ChemMatrix resins utilizing Rink Amide to produce C-terminal amides. For the coupling of amino acids, a pre-activation step was conducted using 5 equivalents of Fmoc-protected amino acid with 4.9 equivalents of *O*-(benzotriazol-1-yl)-*N*,*N*,*N′*,*N′*-tetramethyluronium hexafluorophosphate (HBTU), 5 equivalents of N-hydroxybenzotriazole (HOBt), and 10 equivalents of *N*,*N*-diisopropylethylamine (DIPEA) in Dimethylformamide (DMF), followed by reaction with the N-terminally deprotected peptidyl resin. Thorough washing of the resin with DMF was executed, and the completion of the reaction was assessed using the Kaiser test. Deprotection of Fmoc was achieved with an excess of 20% (v/v) piperidine in DMF, and the washed deprotected peptidyl resin was rinsed with DMF to eliminate any residual piperidine. Cleavage from the resin along with side-chain deprotection occurred using a mixture of 95% TFA, 2.5% TIS, and 2.5% H_2O at room temperature for a duration of 1.5 to 2 hours. The resultant peptide was precipitated using cold diethyl ether, separated via centrifugation, and subsequently dissolved in water containing 0.1% trifluoroacetic acid before undergoing RP-HPLC and ESI-MS analyses.

The reverse complementary sequences of RNA aptamers DNA (RRE, P22N, λN, Pepper, and XBE (Table S8) with T7 promoter were synthesized and annealed with T7 promoter as templates for in vitro transcription. The RNA aptamers were *in vitro* transcribed according to the Transcription T7 kit (Cat. 6140, Takara) and labeled with biotin using Pierce™ RNA Biotin Labelling Kit (Cat. 20160, Thermo Scientific).

EMSA experiments were performed using a LightShift Chemiluminescent RNA EMSA Kit (Cat. 20158, Thermo Scientific). 3′ biotin-labeled RNA probes and Synthesized peptides were incubated in binding buffer (3 mM MgCl2, 40 mM KCl, 5% glycerol, 2 mM DTT, 2 μg tRNA) for 40 min at room temperature, and mobility shift assay was performed using 6% acrylamide native gel electrophoresis. After electrophoresis, Sandwich the gel and 0.5X TBE buffer-soaked nylon membrane in a clean electrophoretic transfer unit for electrophoretic transfer at 400mA (~35V) for 30 minutes. After UV cross-linking, biotin signals were detected with Stabilized Streptavidin-Horseradish Peroxidase Conjugate according to the manufacturer's manual of LightShift Chemiluminescent RNA EMSA Kit.

Design of RNA switches

The RNA switches were designed based on the RRE sequence, containing three functional elements, probe sequence, linker 1, and Linker 2. The linker 1 and linker 2 hybridize with the RRE and the probe, respectively.

Linker2 is designed as the reverse complementary sequence to the 3' end of the RRE legend. Its role is to disrupt the active conformation of the RRE ligand by base-pairing with its 3' end. Therefore, the linker 2 sequence should be placed at the 5' end of the RNA switch, allowing it to hybridize with the 5' end of the RRE ligand, which is critical for maintaining the inactive conformation of the RNA switch. It is worth noticing that the binding strength between Linker2 and the RRE ligand should not be excessively strong. If the binding force is too strong and the change of RRE conformation is completely disrupted, the RRE will not be able to revert to its active conformation, even when the probe binds.

Linker 1 sequences were introduced, which is designed to be reverse complementary to the 3' end of the probe sequence. Its primary function is to enhance the inactive conformation of the RRE by Linker 2 in the absence of the target RNA. In the presence of the target RNA, the probe binds to the target RNA, triggering the dissociation of linker1 from the probe. This dissociation

further disrupts the binding of linker 2 and the RRE ligand, allowing the RRE to regain active conformation.

For the design of the probe, we used the Stellaris Probe Designer on Biosearch Technologies (https://www.biosearchtech.com/support/tools/design-software/stellaris-probe-designer) with default settings. The 5' and 3' UTR regions of target RNAs should be avoided in designing the probe. Additionally, a probe with an annealing temperature below 65°C and a minimum length of 22 nucleotides is desirable.

The structures of RNA switch sequences were predicted by the mFold online tool (website: www.unafold.org/mfold/applications/rna-folding-form.php) with default settings.

Expression of RNA switch-RTF in plants

The plasmid pCambia1300s was used as a backbone to construct RNA switch-RTF components. The sequences encoded for fused GFP-RBP-RRRG proteins were cloned into the plasmid under the pUBQ10 promoter. The sequences of the RNA switch driven by the AtU6 promoter, with various probes targeting mCherry, were cloned in the same plasmid upstream of the pUBQ10 promoter. The RNA switch sequences are listed in Table S9. These types of plasmids were named RNA switch-RTF plasmids (Table S10). These plasmids were introduced into the leaves of *N. benthamiana* mCherry overexpression lines via agroinfiltration.

The RNA switch-RTF plasmid with a probe targeting *CM3* mRNA was introduced into *A. thaliana* wildtype and *cm3* mutant plants respectively via floral dip. Homozygous T3 lines were used.

Design of RTF-SFP and RTF-SunTag

RTF-SFP was modified in the RNA switch-RTF plasmid described above by replacing sequences encoded for fused GFP-Rev-RRRG proteins with the sequences of GFP_{1-10}, an internal ribosome entry site (IRES), and 24×GFP_{11}. These types of plasmids were named RNA switch-RTF-SFP plasmids (Table S10).

RTF-SunTag was also modified in the RNA switch-RTF plasmid, by replacing sequences encoded for fused GFP-Rev -RRRG proteins with sequences of SunTag- Rev, an internal ribosome entry site (IRES), and GFP-scFv-RRRG. These types of plasmids were named RNA switch-RTF-SunTag plasmids (Table S10).

Generation of transgenic *A. thaliana* plants expressing various RNA-Switch-RTFst constructs

A serial of RNA switch-RTF-SunTag (RNA switch-RTFst) plasmids with various probe sequences in RNA switches were constructed (Table S9). These plasmids were introduced to *Agrobacterium tumefaciens* (strain GV3101). Transgenic *A. thaliana* lines were generated via the floral dip method *(2)*, and the homozygous lines were used.

Single-molecule fluorescence *in situ* hybridization

For probe design, five probes targeting various sites of the *CM3* coding region were designed using the online program Stellaris® Probe Designer version 2.0 from Biosearch Technologies (http://singlemoleculefish.com). Before ordering pre-labeled probes from Biosearch Technologies, we completed a TAIR BLAST query for each sequence to ensure target specificity (https://www.arabidopsis.org/Blast/). The oligonucleotides of each probe, labeled with Cy3 at the 5' terminus, were synthesized by Sangon Biotech Co., Ltd..

For sample preparation, root tips of 10-day-old transgenic seedlings were collected and fixed in 2-(N-morpholino) ethane sulfonic acid (MES) buffer, pH 5.7, containing 4% paraformaldehyde for 30 minutes at room temperature. The roots were rinsed twice with 1× PBS and placed onto a microscope slide with a coverslip. They were gently squashed and briefly submerged in liquid nitrogen. The coverslips were then removed, and the samples were left to dry at room temperature for 30 minutes. Tissue permeabilization was carried out by immersing the samples in Coplin jars containing 70% ethanol, which were shaken gently for at least 1 hour. The ethanol was evaporated at room temperature before the roots were washed twice with MES.

Hybridization was performed as previously described (3). Briefly, 100 μL of hybridization solution with probes at a final concentration of 250 nM was added to each slide. Coverslips were placed over the samples to prevent buffer evaporation, and the probes were left to hybridize in a humid chamber at 37°C overnight in the dark. The samples were washed twice for 45 minutes at 37°C with freshly prepared 1×SSC/40% formamide buffer, rinsed at room temperature with MES buffer (pH 5.8), and dried. A drop of ProLong Diamond Antifade Mountant (Invitrogen) containing DAPI was added prior to observation.

Construction of MCP-MS2 system

The DNA sequence of 24×MS2 were cloned to 3'UTR of *CM3* under control of pUBQ10 promoter to form a fused CM3-24×MS2-expressing plasmid. The DNA encoded for fused mCherry-MCP protein was cloned into the plasmid under the pUBQ10 promoter.

Protoplast isolation and imaging

Agrobacterium containing RNA switch-RTF-SunTag plasmids were co-transformed into tobacco epidermal cell with that containing CM3-24×MS2 plasmid and mCherry-MCP plasmid by Agroinfiltration of *N. benthamiana* assay as described above. 28 hours after infiltration, the leaves were cut off for protoplast isolation based on described previously protocol. Images were taken using a Leica SP5 X MP confocal microscope using a×40 Leica objective, with excitation and emission at 488 and 509 nm for GFP, and 575 and 650 nm for mCherry.

Estimating the proximity of RNAs to mitochondria

N. benthamiana leaves were agroinfiltrated with constructs expressing RNA switch-RTF-SunTag and mitochondrial-targeting RNA *VDAC3*. 28 hours after infiltration, leaves were infiltrated with 1μM MitoTracker® Red CMXRos (ThermoFisher, A66443) for Mitochondria Labeling. The movements of *VDAC3* RNA particles to mitochondria in living epidermal cells of *N. benthamiana* were captured using confocal microscopy time-lapse imaging. The distance from the center of each *VDAC3* RNA particle to the center of the closest mitochondrion is measured with ImageJ and the number of particles at a given mitochondrion distance is calculated (*4*).

Western blotting

Total plant protein extraction and western blotting were performed as previously described (*5*). Briefly, protein extracts were mixed with sodium dodecyl sulfate-polyacrylamide gel electrophoresis (SDS-PAGE) sample buffer and denatured at 95 °C for 5 min. After brief centrifugation, denatured protein samples were separated by 12% SDS-PAGE and blotted onto PVDF membranes. Primary and secondary antibodies were used at the following dilutions: 1:10,000 for GFP (ab290; Abcam), 1:10,000 for ubiquitin (MAB3408; Sigma-Aldrich), and 1:10,000 for anti-IgG (mouse) HRP conjugate (W402B; Promega). Immunoreactive bands were visualized using ImmunoStar® LD (Wako). The molecular weights were estimated using the ExPASy SIB bioinformatics resource portal.

Microscopy setup and image acquisition

For protoplast imaging, protoplasts were stained with 100 μM FM4-64 for 1 min and washed with W5 solution before imaging. For leaf epidermal cell imaging, agroinfiltrated *N. benthamiana* leaves were cut for imaging 72 hours after agroinfiltration. For mitochondrial localization, agroinfiltrated leaves were incubated with 200 nM MitoTracker red CMXRos in 1×PBS buffer with 3% (w/v) Sucrose for 15 min before imaging (*6*). Images were captured on a spinning disk confocal microscope (Olympus SpinSR10) with an EMCCD camera and ×40 oil objective. GFP,

Cy3, DAPI, FM4-64 and MitoTracker red CMXRos signals were detected at respective excitation/emission wavelengths of 488/498-559 nm, 554/568 nm, 405/420-480 nm, 488/734 nm and 561 nm/580–625 nm. Panoramic images of tissues were acquired with the Olympus VS200 panoramic digital scanner (Olympus Corp., Tokyo, Japan). For visualization of *TUB5* expression during plant growth, the GFP signal in whole plants was acquired using NightShade LB 985 In vivo Plant Imaging System (Berthold) every two weeks throughout the growth period. For detection of *AtTCTP1* mRNA long-distance movement, the rootstock samples at different distances from the grafting junction were cut for Z-stack image acquisition using a spinning disk confocal microscope (Olympus SpinSR10) with an EMCCD camera and ×20 objective. For observation of the cell-to-cell movement of *AtTCTP1* mRNA, time-lapse imaging of elongation region cells of rootstock root was performed using a SpinSR10 microscope with a ×20 objective every 3 sec for 1 min.

RT-qPCR

Total RNA was extracted using the Qiagen RNeasy kit, following the manufacturer's instructions. Reverse transcription was performed using the Qiagen Omniscript kit with a primer mix of random 10mers (final concentration of 10 μM) and 15mer oligo dT primers (final concentration of 1 μM). A negative control was performed by adding water instead of reverse transcriptase. mRNA abundance was calculated using the $2^{-\Delta\Delta Ct}$ method. A negative control experiment was performed under identical conditions, replacing the reverse transcriptase enzyme with water. Primers were listed in Table S7.

Micro-grafting of *A. thaliana* plants

A. thaliana seeds were vertically grown on plates containing 1/2 MS salts, 1% sucrose, and 1% micro agar under short-day conditions in a controlled environmental chamber (Percival) for one week. Micro-grafting of *A. thaliana* seedlings was performed as described (*7*). Briefly, Seedlings of similar size and with evenly elongated hypocotyls were cut in the upper half of the hypocotyl with a sterilized razor blade. The junctions of the graft were supported using silicon microtubing (0.3 mm internal diameter). Grafted plants were then transferred to new plates and grown vertically under short-day conditions. Adventitious roots that formed above the junction were removed every two days.

Aphid feeding experiments

Ya1-targeted RNA switch-RTFst plasmids were agroinfiltrated into four-week-old *N. benthamiana* leaves. 48 hours post-infiltration, approximately 5 aphids were confined to the infiltration zone using rubber bands and double-sided tape to prevent escape. After 24 hours of feeding, leaf samples were collected for confocal fluorescence microscopy using an Olympus FV3000. Additionally, co-infiltration of full-length *Ya1* plasmids with *Ya1*-targeted RNA switch-RTFst plasmids was performed.

Leaf discs (4 cm^2) containing agroinfiltrated switch-RTFst plasmid constructs were excised 48 hours post-infiltration and transferred to six-well plates containing Murashige and Skoog (MS) liquid medium to maintain osmotic balance and humidity. Aphids (3–4 individuals) were introduced onto the leaf discs, followed by incubation in controlled growth chambers (25°C, 16/8 h light/dark). Time-lapse imaging was conducted at hourly intervals using an Olympus SpinSR10 spinning disk confocal microscope, equipped with an automated stage scanning system for panoramic imaging.

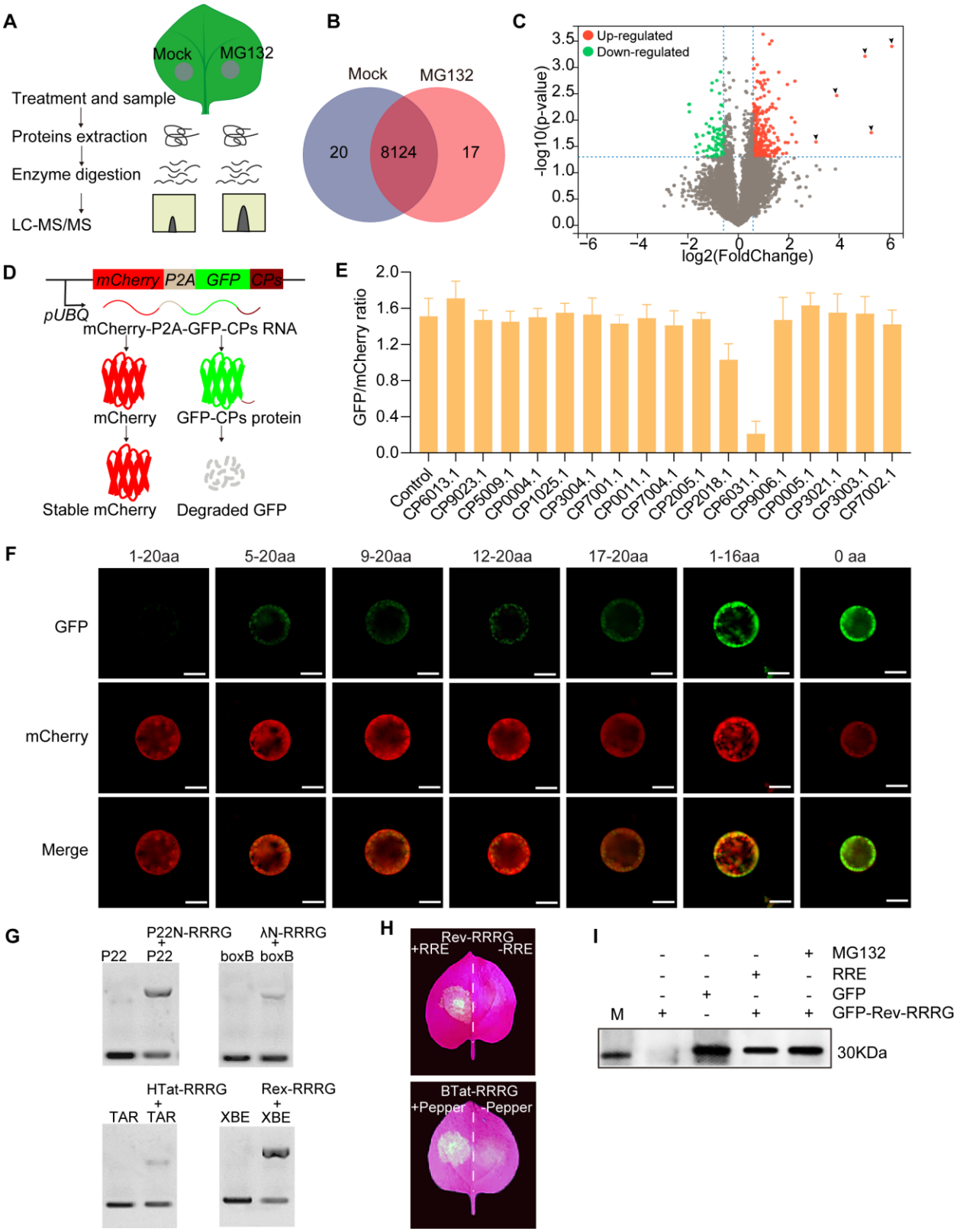

Fig S1. *de novo* identification of degrons. (A) Flowchart showing the identification of

constitutively degraded proteins. *N. benthamiana* epidermal cells were infiltrated wither with 10 μM MG132 for 24 hours to inhibit proteasome activity or 1×PBS buffer (mock), followed by protein extraction and LC-MS/MS analysis. **(B)** 17 proteins were identified in *N. benthamiana* leaves treated with MG132 compared to those treated with the mock groups. **(C)** Volcano plot illustrating differentially abundant proteins. **(D)** Schematic of representation of the co-expression system used for fluorescence normalization of GFP fusions. mCherry and GFP, tagged with the putative degron sequence, were co-expressed using a 2A self-cleaving peptide system. CP represents the 20 aa at the C-terminal of 17 proteins detected in MG132-treated leaves. **(E)** Assessment of the effect of CP on the GFP degradation based on the GFP/mCherry fluorescence intensity ratio. **(F)** Representative image showing the effect of different truncations of CP6031.1 on GFP degradation. The scale bar indicates 20 μm. **(G)** The gel-shift assay testing RNA binding ability of RBP tagged with the RRRG degron. **(H)** GFP fluorescence signals in the presence and absence of specific RNA aptamers when BTat and Rev tagged with RRRG. *N. benthamiana* leaves were imaged at three days post-agroinfiltration. **(I)** Western blot detection of GFP protein.

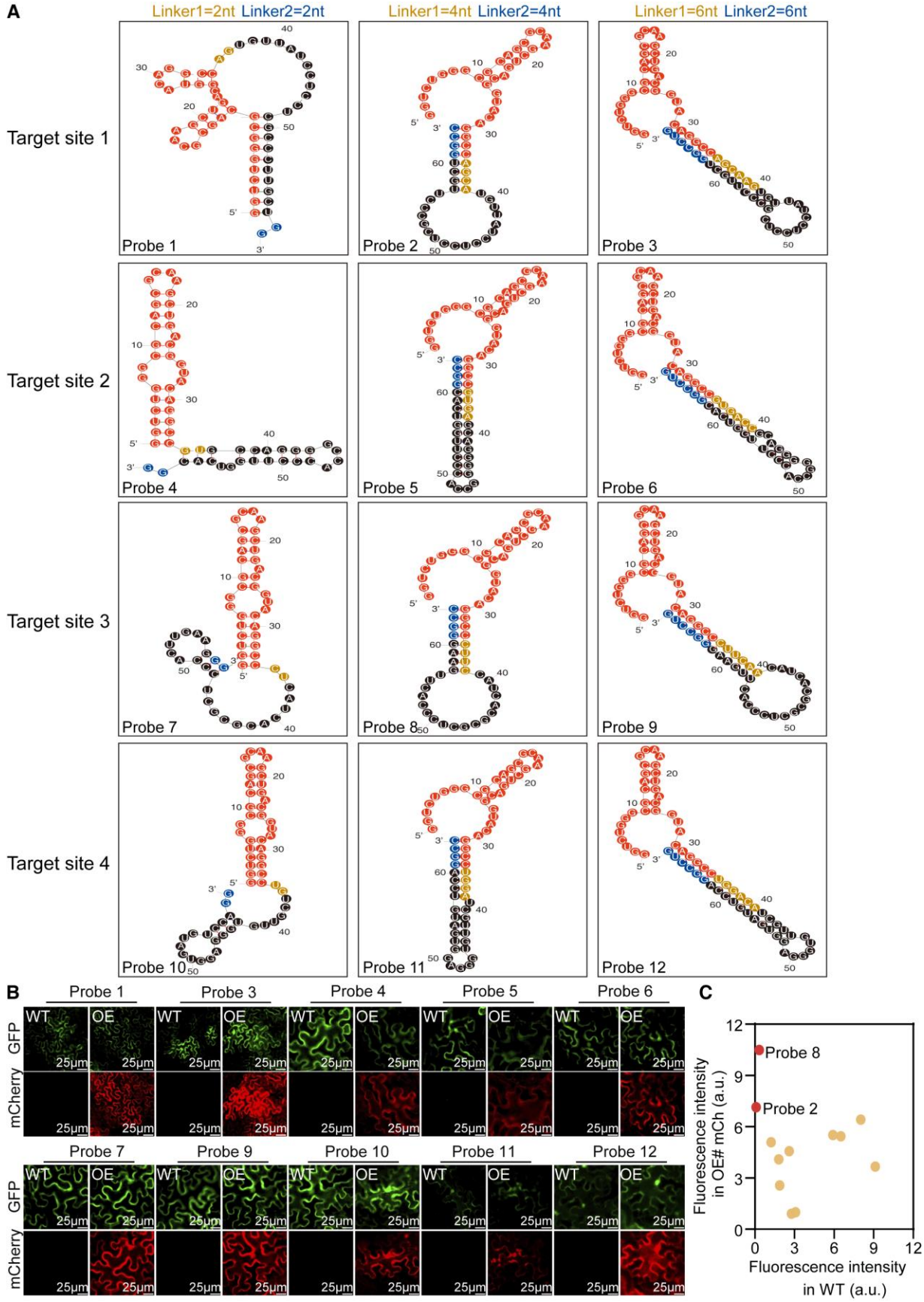
A
Linker1=2nt Linker2=2nt
Linker1=4nt Linker2=4nt
Linker1=6nt Linker2=6nt
Target site 1
Target site 2
Target site 3
Target site 4
Probe 1
Probe 2
Probe 3
Probe 4
Probe 5
Probe 6
Probe 7
Probe 8
Probe 9
Probe 10
Probe 11
Probe 12
B
Probe 1
Probe 3
Probe 4
Probe 5
Probe 6
Probe 7
Probe 9
Probe 10
Probe 11
Probe 12
GFP
mCherry
WT
OE
25μm
C
Probe 8
Probe 2
Fluorescence intensity in OE# mCh (a.u.)
Fluorescence intensity in WT (a.u.)
0
3
6
9
12

Fig S2. Designing of RNA switches targeting mCherry RNA. (A) Minimal free energy (MFE) secondary structure of 12 RNA switches (Probe1-12) designed for specifical targeting *mCherry*. The RNA switches feature linker lengths ranging from 2 to 6 nt. **(B)** Screening of RNA switches using fluorescent microscopic images of *N. benthamiana* epidermal cells. Scale bars indicate 50μm. **(C)** Fluorescence quantification of 12 RNA-switches to control RTF reporter in WT and *mCherry*-expressing epidermal cells of *N. benthamiana* leaves.

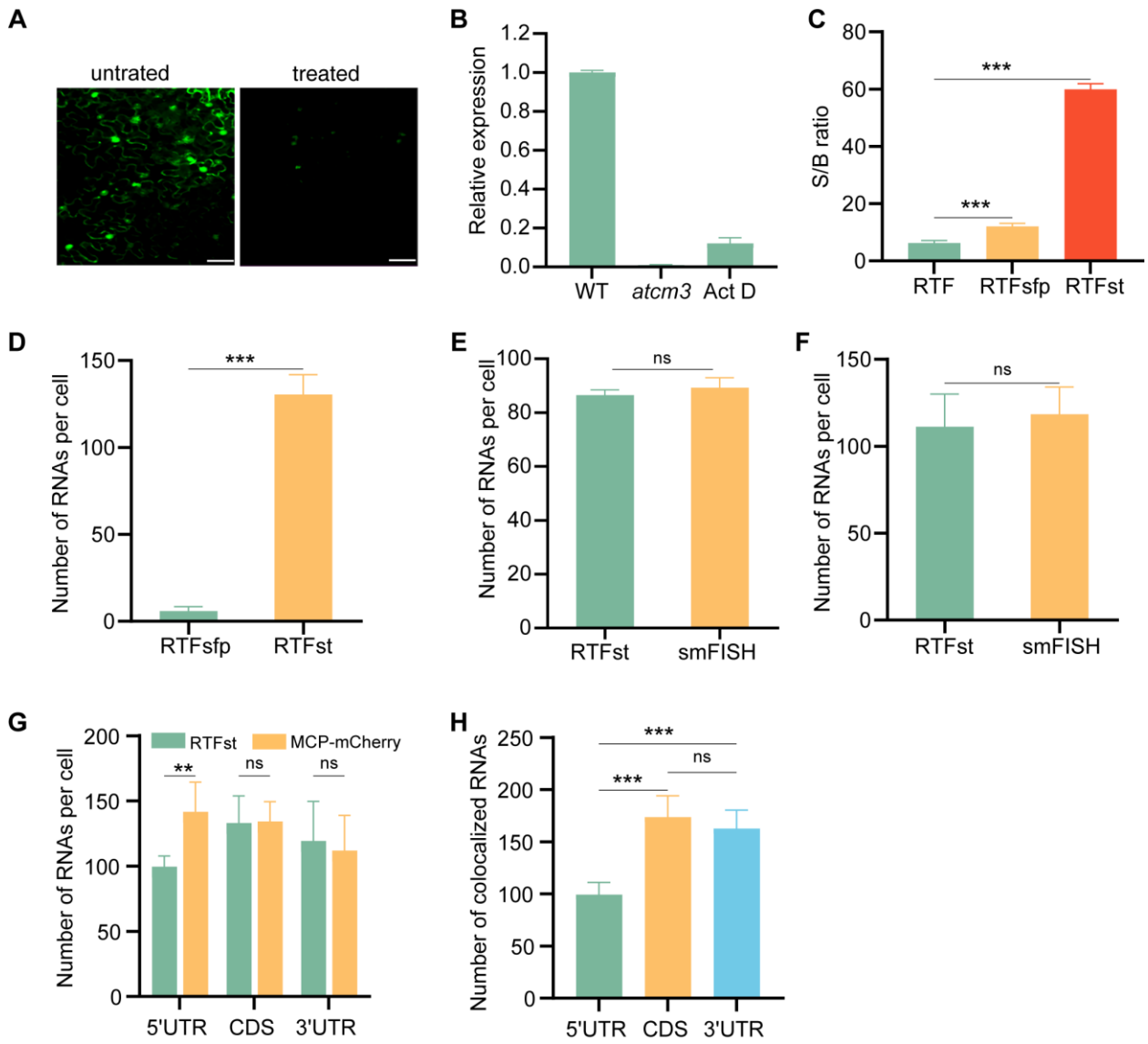

Fig S3. Expression of RNA switch-controlled RTF system in plants. (A and **B)** The RNA switch-RTF system exhibited a degree of leakage in the absence of the target RNA. **(A)** Fluorescence imaging of *N. benthamiana* leaf epidermal cells expressing the RNA switch-RTF system targeting *CM3* mRNA. "Untreated" indicates cells not exposed to Actinomycin D (Act D), an RNA synthesis inhibitor, while "treated" indicates cells subjected to Act D treatment. Scale bars: 25 μm. **(B)** Relative expression levels of *CM3* mRNA in wild-type (WT), *cm3* mutant, and Act D-treated WT plants. **(C)** Quantification of the signal-to-noise ratio (SNR) for RTF, RTF-SFP, and RTF-SunTag in *cm3* mutants (n = 6, mean ± s.e.m., *** $P < 0.001$, two-tailed unpaired Student's t-test). **(D)** The number of well-dispersed diffraction-limited fluorescent puncta per cell (n=6, mean ± s.e.m., **** $P<0.001$, two-tailed unpaired Student's t-test). **(E** and **F)** Quantification

of *CM3* mRNA in individual root **(E)** and leaf **(F)** cells using smFISH and the RNA switch-RTFst system. Statistical comparisons for root cells (n = 6, mean ± s.e.m., $P > 0.05$, not significant [ns], two-tailed unpaired Student's t-test) and leaf cells (n = 6, mean ± s.e.m., $P > 0.05$, ns, two-tailed unpaired Student's t-test). **(G)**. Quantification of *CM3* mRNA detected by the RNA switch-RTFst system and the mCherry-MCP-MS2 system (n = 6, mean ± s.e.m., ns, $P > 0.05$; $P < 0.01$, two-tailed unpaired Student's t-test). **(H)** Number of colocalized *CM3* mRNAs detected by the RNA switch-RTFst system and the mCherry-MCP-MS2 system (n = 6, mean ± s.e.m., ***$P < 0.001$, two-tailed unpaired Student's t-test).

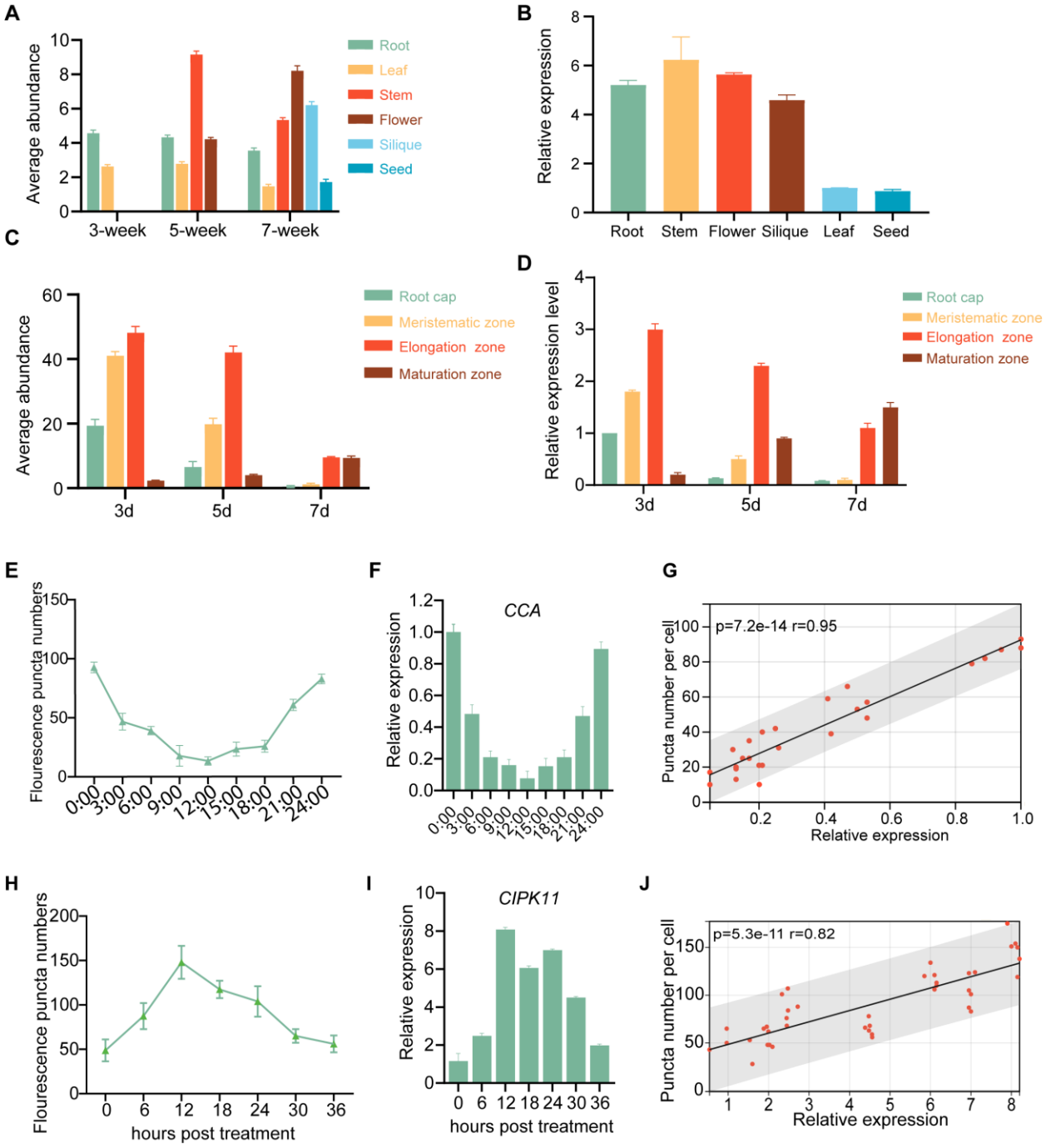

Fig. S4. Quantification of RNA abundance using the RNA switch-RTFst system in living plants. (A) Average abundance of *TUB5* in different tissues, as measured by the RNA switch-RTFst system. **(B)** Relative expression levels of *TUB5* in different tissues of 7-week-old *A. thaliana* seedlings, assessed by RT-qPCR. **(C)** Average abundance of *SMB* in root tip tissues, as revealed by the RNA switch-RTFst system. **(D)** Relative expression levels of *SMB* in root tip

tissues, assessed by RT-qPCR at 3, 5, and 7 days after germination. **(E** and **F)** Average abundance of *CCA1* in leaves of 7-week-old *A. thaliana* over a 24-hour period, as quantified by the RNA switch-RTFst system **(E)** and RT-qPCR **(F)**. **(G)** Correlation between *CCA1* expression levels measured by the RNA switch-RTFst system and RT-qPCR. **(H** and **I)** Average abundance of *CIPK11* in roots of 7-week-old Arabidopsis under cadmium (Cd) stress, as determined by the RNA switch-RTFst system **(H)** and RT-qPCR **(I)**. **(J)** Correlation between *CIPK11* expression levels measured by the RNA switch-RTFst system and RT-qPCR.

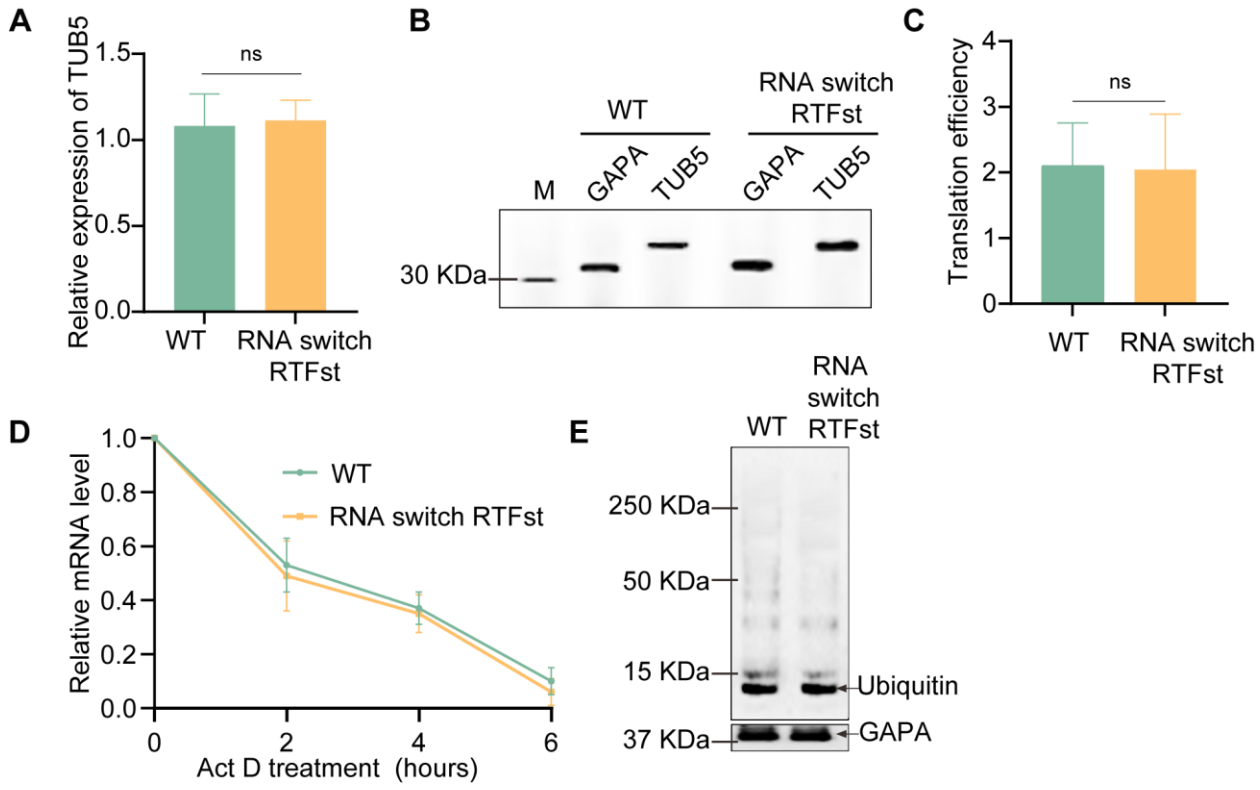

Fig. S5. The fate of *TUB5* mRNA in Arabidopsis thaliana is unaffected by the RNA switch-RTFst system. (A) Relative expression levels of *TUB5* mRNA in wild-type (WT) plants and *A. thaliana* plants expressing the RNA switch-RTFst system (n = 9, mean ± s.e.m., ns, not significant, $P > 0.05$, two-tailed unpaired Student's t-test). **(B)** Levels of TUB5 protein in WT plants and *A. thaliana* plants expressing the RNA switch-RTFst system. GLYCERALDEHYDE 3-PHOSPHATE DEHYDROGENASE A SUBUNIT (GAPA) was used as an internal reference. **(C)** Translation efficiency of *TUB5* mRNA in WT plants and *A. thaliana* plants expressing the RNA switch-RTFst system. Translation efficiency was calculated by normalizing TUB5 protein levels to *TUB5* mRNA levels (n = 9, mean ± s.e.m., ns, not significant, $P > 0.05$, two-tailed unpaired Student's t-test). **(D)** Degradation dynamics of *TUB5* transcripts following Act D treatment in the roots of WT and *A. thaliana* plants expressing the RNA switch-RTFst system. One-week-old *A. thaliana* seedlings were treated with 20 μM Act D, and relative *TUB5* transcript levels were quantified by RT-qPCR at 0, 2, 4, and 6 hours post-treatment. **(E)** Overall ubiquitination patterns were similar in WT plants and *A. thaliana* plants expressing the RNA switch-RTFst system. GAPA protein was used as an internal reference.

Table S1 20 aa at the C-terminal of 17 proteins detected in MG132-treated *N. benthamiana* leaves. The reference proteins of *N. bentamiana* were download from Sol Genomics Network database (https://solgenomics.net/ftp/genomes/Nicotiana_benthamianaV261/Nbenthamiana_Annotation/).

Proteins	C-terminal peptides (CPs) name	Amino acid sequence	Gene ID
Niben261Chr01g0596013.1	CP6013.1	WSSDHIALLAEFRCKPRTRR	107761103
Niben261Chr04g1859023.1	CP9023.1	NIFPLWGLAEYRKNVLLQNY	107770515
Niben261Chr06g0625009.1	CP5009.1	LDKPGFVPLLTAHMAGGLNV	107791570
Niben261Chr09g1100004.1	CP0004.1	KDGVHFHHFKDGKCSCCDFW	107760323
Niben261Chr10g0111025.1	CP1025.1	KWGCPVCRANIDQVIRLYAV	107777805
Niben261Chr12g0313004.1	CP3004.1	KLVYRFSSSSFGRAKNNDIP	107791192
Niben261Chr12g0827001.1	CP7001.1	FRDNDYIDILPKDIQPSRGT	107781174
Niben261Chr12g0990011.1	CP0011.1	TKVKQIYVAKQTISGTKTTG	107816357
Niben261Chr14g0257004.1	CP7004.1	LAGEAKMLCRDIAGHVEFFR	107827605
Niben261Chr14g1162005.1	CP2005.1	SRLVETGSSDQLDIGKPMIN	107782682
Niben261Chr17g0072018.1	CP2018.1	LLLKKFMKANGLGAVFMDES	107775987
Niben261Chr17g1266031.1	CP6031.1	ITHNVTSVDIQNAIVERRRG	107826966
Niben261Chr07g0989006.1	CP9006.1	MEGKFELWGLNYGLSHPHYV	107767796
Niben261Chr10g0130005.1	CP0005.1	GRVFVVVNWKLIVRDTPSMG	107761493
Niben261Chr04g0243021.1	CP3021.1	EKHFGLFSPDQRAKYQLNFN	107763289
Niben261Chr08g0313003.1	CP3003.1	LALTNQPFIVFFRKFQKTDG	107799889
Niben261Chr06g1467002.1	CP7002.1	LAEEAKTLAAALLEEEIMDN	107831752

Table S2 Information on RNA-binding polypeptide (RBP) and RNA aptamers. The red font indicates shared amino acid residues between ARM and RRRG degron.

Name	Sequences with degron (RRRG)	RBP	Sequences	RNA ligands	Reference
Rev-RRRG	TRQARRNRRRRWRE**RRRG**	HIV-1 Rev	TRQARRNRRRRWRERQR	RRE	(*8*)
P22N-RRRG	NAKTRRHERRRKLAIE**RRRG**	P22N	NAKTRRHERRRKLAIER	P22 boxB	(*9*)
λN-RRRG	MDAQTRRRE**RRRG**	λN	MDAQTRRRERRAEKQAQWKAAN	boxB	(*10*)
BTat-RRRG	SGRSRRSRGTRGKGRRIR**RRG**	BIV-Tat	SGRSRRSRGTRGKGRRIRR	Pepper	(*11*)
HTat-RRRG	SYGRKKRRQ**RRRG**	HIV-Tat	SYGRKKRRQRRRRSRSQ	HIV-1 TAR	(*12*)
Rex-RRRG	MPKTRRRPRRSQRK**RRRG**	HTLV-1 Rex	MPKTRRRPRRSQRKRP	XBE	(*13*)

Table S3 RNA switches for imaging mCherry RNA. The red, brown, black and blue font indicates respectively the RRE aptamer, linker 1, the probe sequence, and linker 2 in RNA switches.

Target sites	RNA switch (RS) name	Sequences
AGCAAGGGCGAGGAGGAUAACA	RS#1	GGUCUGGGCGCAGCGCAAGCUGACGGUACAGGCCAGUGUUAUCCUCCUCGCCCUUGCUGG
	RS#2	GGUCUGGGCGCAGCGCAAGCUGACGGUACAGGCCAGCAUGUUAUCCUCCUCGCCCUUGCUGGCC
	RS#3	GGUCUGGGCGCAGCGCAAGCUGACGGUACAGGCCAGCAAGUGUUAUCCUCCUCGCCCUUGCUGGCCUG
UGGCCAUCAUCAAGGAGUUCAU	RS#4	GGUCUGGGCGCAGCGCAAGCUGACGGUACAGGCCGTGCAGGGGGCCACCCUUGGUCACGG
	RS#5	GGUCUGGGCGCAGCGCAAGCUGACGGUACAGGCCGUGAGCAGGGGGCCACCCUUGGUCACGGCC
	RS#6	GGUCUGGGCGCAGCGCAAGCUGACGGUACAGGCCGUGACCGCAGGGGGCCACCCUUGGUCACGGCCUG
UUCAAGUGGGAGCGCGUGAUG	RS#7	GGUCUGGGCGCAGCGCAAGCUGACGGUACAGGCCCUCAUCACGCGCUCCCACUUGAAGGG
	RS#8	GGUCUGGGCGCAGCGCAAGCUGACGGUACAGGCCCUUCCAUCACGCGCUCCCACUUGAAGGGCC
	RS#9	GGUCUGGGCGCAGCGCAAGCUGACGGUACAGGCCCUUCAACAUCACGCGCUCCCACUUGAAGGGCCUG
UCGUUGUGGGAGGUGAUGUCCA	RS#10	GGUCUGGGCGCAGCGCAAGCUGACGGUACAGGCCUGUCGUUGUGGGAGGUGAUGUCCAGG
	RS#11	GGUCUGGGCGCAGCGCAAGCUGACGGUACAGGCCUGGAUCGUUGUGGGAGGUGAUGUCCAGGCC
	RS#12	GGUCUGGGCGCAGCGCAAGCUGACGGUACAGGCCUGGACAUCGUUGUGGGAGGUGAUGUCCAGGCCUG

Table S4 smFISH probes used for targeting *CM3* mRNA

Probes	Sequences (5'-3')	5'-labeling
Probe 1	aacgcgggtttgagtaacttag	Cy3
Probe 2	aatcgcgagatgagtcttgaag	Cy3
Probe 3	aggaagagagacccagaagata	Cy3
Probe 4	aaatactcactctcatctaccc	Cy3
Probe 5	aagataatactgtcctcttgac	Cy3
Probe 6	aagataatactgtcctcttgac	Cy3
Probe 7	tttcagtttctctgaccataaa	Cy3
Probe 8	taggaggaaggataggttcagg	Cy3
Probe 9	taggaggaaggataggttcagg	Cy3
Probe 10	ctgaaccacaattaccgtcatc	Cy3

Table S5 Specific probe sequences targeting the 5'UTR, CDS, and 3'UTR of *CM3* mRNA.

Probes	Sequences (5’-3’)
$P_{5'UTR}$	AGAGACAGAGACAGAGAGTGGA
P_{CDS}	CAAATACTCACTCTCATCTACC
$P_{3'UTR}$	AAATGTTATGCTTCCTTCTTTG

Table S6 Information of target genes.

Gene name	Locus	Gene ID
TUB5	AT1G20010	838590
CCA1	AT2G46830	819296
CIPK11	AT2G30360	817586
SMB	AT1G79580	844296

Table S7 Primers for genotyping of Arabidopsis mutants and RT-qPCR.

Purposes	Genes	Forward primers	Reverse primers	T-DNA Left border primers
Genotyping identification	*cm3*	LP: TGTGGGGTCAGGAATTTAATG	RP: AAGAAAAGGACAGAGGAACGG	LB: ATTTTGCCGATTTCGGAAC
	tctp1	CAAGCAAGATACGATAGATTGGGGT	TAACCTTTCAGGATCAGGCTGAGG	ATAATAACGCTGCGGACATCTACATTTT
RT-qPCR	*CM3*	TCCCCAAACCTCAATCTTAC	ACTCACTCTCATCTACCCTT	
	CIPK11	CAGATCAAGTTCCACGATGA	CCCGACGAGTAAGAAATCAA	
	CCA1	AAGGTGGACTGAGGAAGAACATA	AGCCTCTTTCTCTACCTTGGA	
	TCTP1	AAGGAAAGTGGGTTACTGTG	TAAGTTGGTTGCTCCTGAAG	
	VDAC3	TTCACGACCAAAGAGAACG	TGAAGAACGACTTTGGACG	
	Ya1	ACAAGTCCAATCTGCCAAG	ACTGATTTATTTTGCGGTGG	
	SMB	GTCCTCAAAACGAGTGGTAT	CTTCTTGGAGCTGTTGAGAT	
	TUB5	TCGTCTTACTTCGTTGAGTG	TCCATTCCTTCTCCTGTGTA	

Table S8 DNA sequences for *in vitro* transcription of RNA aptamers. Lowercase letters indicate the reverse complementary sequence of the T7 promoter.

RNA aptamers	DNA sequences of RNA aptamers	Reverse complementary sequences for *in vitro* transcription
RRE	GGCTCGTGTAGCTCATTAGCTCCGAGCC	GGCTCGGAGCTAATGAGCTACACGAGCCcctatagtgagtcgtatta
P22 boxB	GGTGCGCTGACAAAGCGCGCC	GGCGCGCTTTGTCAGCGCACCcctatagtgagtcgtatta
boxB	GGGCCTGAAGAAGGGCCC	GGGCCCTTCTTCAGGCCCcctatagtgagtcgtatta
BIV TAR	GGCTCGTGTAGCTCATTAGCTCCGAGCC	GGCTCGGAGCTAATGAGCTACACGAGCCcctatagtgagtcgtatta
HIV-1 TAR	CCAGATCTGAGCCTGGGAGCTCTCTGG	CCAGAGAGCTCCCAGGCTCAGATCTGGcctatagtgagtcgtatta
XBE	GCTCAGGTCGAGGTACGCAAGTACCTCCCTTGGAGC	GCTCCAAGGGAGGTACTTGCGTACCTCGACCTGAGCcctatagtgagtcgtatta

Table S9 Probe sequences in RNA switch for imaging target gene expression.

Genes	Probe sequences
SMB	ATTCTGCATTTCTCTTTAAGTT
CCA1	GGGAGGCCAAAATGATGAGGCG
CIPK11	CTCTTCCTCCTTCTTCTTCTTC
TCTP1	TAATGTAAGCGATGAATCCCTT
Ya1	CGGACTCCTTTATATACACT

Table S10 Information of plasmids used in this study.

Type	Plasmid name	Purposes
RNA switch-RTF	pcambia1300-Ubq10-RTF	Expressing RTF
	pcambia1300-RSmCherry-RTF	Imaging mCherry RNA using RNA switch and RTF
	pcambia1300-RSCM3-RTF	Imaging CM3 RNA using RNA switch and RTF
RNA switch-RTF-SFP	pcambia1300-24XGFP11	Expressing 24XGFP11
	pcambia1300-RSCM3-GFP1-10	Expressing RSCM3 and GFP1-10
RNA switch-RTFst	pcambia1300-RSVDAC3-RTFst	Imaging VDAC3 RNA using RNA switch and RTFst
	pcambia1300-RSTUB5-RTFst	Imaging TUB5 RNA using RNA switch and RTFst
	pcambia1300-RSCM3-RTFst	Imaging CM3 RNA using RNA switch and RTFst
	pcambia1300-RSCIPK11-RTFst	Imaging CIPK11 RNA using RNA switch and RTFst
	pcambia1300-RSCCA1-RTFst	Imaging CCA1 RNA using RNA switch and RTFst
	pcambia1300-RSTCTP1-RTFst	Imaging TCTP1 RNA using RNA switch and RTFst
	pcambia1300-RSVDAC3-RTFst	Imaging VDAC3 RNA using RNA switch and RTFst
	pcambia1300-RSYa1-RTFst	Imaging RSYa1 RNA using RNA switch and RTFst
SM2-MCP system	pcambia1300-24×MS2	Expressing 24×MS2
	pcambia1300-mCherry-MCP	Expressing mCherry-MCP

References

1. V. Demichev, C. B. Messner, S. I. Vernardis, K. S. Lilley, M. Ralser, DIA-NN: neural networks and interference correction enable deep proteome coverage in high throughput. *Nat. Methods* **17**, 41-44 (2020).
2. S. J. Harrison *et al.*, A rapid and robust method of identifying transformed seedlings following floral dip transformation. *Plant Methods* **2**, 1-7 (2006).
3. N. Tsanov *et al.*, smiFISH and FISH-quant - a flexible single RNA detection approach with super-resolution capability. *Nucleic Acids Res.* **44**, 1-11 (2016).
4. M. Michaud *et al.*, Differential targeting of VDAC3 mRNA isoforms influences mitochondria morphology. *P. Natl. Acad. Sci. USA* **111**, 8991-8996 (2014).
5. C. Y. Li *et al.*, Rice stripe virus activates the bZIP17/28 branch of the unfolded protein response signalling pathway to promote viral infection. *Mol. Plant Pathol.* **23**, 447-458 (2022).
6. Z. Yang *et al.*, RNase H1 Cooperates with DNA Gyrases to Restrict R-Loops and Maintain Genome Integrity in Arabidopsis Chloroplasts. *Plant Cell* **29**, 2478-2497 (2017).
7. Y. S. Lai *et al.*, Systemic signaling contributes to the unfolded protein response of the plant endoplasmic reticulum. *Nat. Commun.* **9**, 1-11 (2018).
8. J. L. Battiste et al., Alpha helix-RNA major groove recognition in an HIV-1 Rev peptide-RRE RNA complex. *Science* **273**, 1547-1551 (1996).
9. R. J. Austin, T. Xia, J. Ren, T. T. Takahashi, R. W. Roberts, Designed arginine-rich RNA-binding peptides with picomolar affinity. *J. Am. Chem. Soc.* **124**, 10966-10967 (2002).
10. P. Legault, J. Li, J. Mogridge, L. E. Kay, J. Greenblatt, NMR Structure of the Bacteriophage λ N Peptide/boxB RNA Complex: Recognition of a GNRA Fold by an Arginine-Rich Motif. *Cell* **93**, 289-299 (1998).
11. J. D. Puglisi, L. Chen, S. Blanchard, A. D. Frankel, Solution Structure of a Bovine Immunodeficiency Virus Tat-TAR Peptide-RNA Complex. *Science* **270**, 1200-1203 (1995).
12. C. A. Smith, V. Calabro, A. D. Frankel, An RNA-Binding Chameleon. *Mol. Cell* **6**, 1067-1076 (2000).
13. F. Jiang et al., Anchoring an extended HTLV-1 Rex peptide within an RNA major groove containing junctional base triples. *Struct. Fold. Des.* **7**, 1461-1472 (1999).

Movie S1 Cell-to-cell trafficking of *TCTP1* mRNA in Arabidopsis root.

https://figshare.com/s/fe9495c7145bb9439920

Movie S2 Visualization of aphid-secreted *Ya1* in *N. benthamiana* leaves.

https://figshare.com/s/4f4b7bb5b38c117db768